A MAGNETIC SURVEY OF LOCAL GRAVITY HIGHS IN MAGADI AREA

By

GITHIRI JOHN GITONGA

B.Ed Sc (Hons)

A thesis submitted as partial fulfillment for the award of Master of Science Degree of Kenyatta University.

Faculty of Science
Department of Physics

AUGUST, 1999

DECLARATION

I Githiri John Gitonga, hereby declare that this is my own work and has not been presented for a degree at any other University.

All sources of information have been specifically acknowledged by means of references.

GITHIRI JOHN GITONGA.

This thesis has been submitted with our approval as University supervisors.

DR. RAIMUND L. STANGL

28-02-99

DR. E.W DINDI

DR. I.V.S RATHORE

ACKNOWLEDGEMENTS

I gratefully acknowledge my supervisor Dr. Raimund Stangl for his guidance and support throughout the course of my research. He was a source of constant encouragement and I benefited much from his experience both in the field and of broad knowledge in geophysical prospecting methods. I also wish to thank him for taking his own time to introduce me to pascal programming and for preparing interpretation programs MAGCALC and DEGREC that I used in my work. I also wish to thank my other supervisors Dr. I.V.S Rathore and Dr E.W Dindi for their keen interest in my work. They were quite understanding and encouraged me throughout my work.

I wish also to thank particularly Mr Waithaka and Mr Kadima for the company in the field and many useful discussions we had as M.Sc scholars in geophysics. I also acknowledge Messrs Ngaruiya and Hashim for their continuous encouragement. Thanks are also due to the staff of National Oil Corporation and Ministry of Energy from whose database I greatly benefited in form of data and literature relevant in my work.

My entire Master of Science course was financed by Kenyatta University through Government of Kenya scholarship. I gratefully acknowledge their generosity in being a beneficiary of their scholarship scheme. I also wish to thank all staff members of Physics Department, Kenyatta University for the moral support and assistance they granted me in form of field equipment and materials for this research.

All thanks be to God Almighty the creator of the heavens and earth who was and he is. May all the praise, glory, wisdom, thanks, power and strength be to him forever and ever, Amen.

DEDICATION

This work is dedicated to my dear parents Mr and Mrs Githiri, my dear brothers and sisters and my dear wife Mercy. All your love and generosity are marked in my heart forever. To all I say God bless you.

Abstract

Magadi area is located in the southern part of the Kenya Rift, an active continental rift that is part of the East African Rift system. Thermal manifestations in form of hot springs in northern and southern shores of lake Magadi and high heat flow suggests geothermal potential in the area. The area is highly characterized by grid faults, which allow escape of underground water as hot springs.

A ground magnetic survey have been carried out in this area as a follow-up to investigate whether the known gravity highs at Magadi mapped in the Kenya Tertiary Rift study are related to a heat source responsible for the numerous hot springs. The vertical magnetic field intensity has been measured with a flux-gate magnetometer with an accuracy of ± 2nT. The field has been corrected for both the diurnal and geomagnetic variations and the residual anomaly isolated from the regional. Positioning was carried out by use of a Global Positioning System device. With the reduced magnetic data regularized in a rectangular grid, a contour map was computed to obtain the intensity of the field. Qualitative and quantitative interpretations has been made from the reduced vertical magnetic intensity contour map of the area. Qualitative interpretation involved discerning anomalous regions in the study area from the contour map of the reduced vertical magnetic intensity.

Quantitative interpretation involved both direct interpretation and forward modeling along three selected profiles. The causative bodies are interpreted to have prismatic shapes suggesting them to be dikes. Interpretation involved fitting a calculated model of a thick

sheet assuming uniform magnetization to the observed data by computer iterations. Magnetic bodies at depths of 1 km, 1.09 km, 0.9 km and 1.0 km with widths of 2.2 km, 3.5 km, 1.5 km and 1.0 km. Their dips are 78°, 40°, 60° and 105° with strike directions as 150°, 83°, 144° and 144° respectively. The depths to the bottom of bodies are 1.99 km, 4.09 km, 3.0 km and 2.9 km respectively. These depths to the bottom where the bodies cease to be magnetic are considered shallow suggesting the depths to represent Curie point depth. The models obtained are considered reasonable as they match well with the geology of the area and with other geophysical studies that had been carried out in the research area.

Contents Page

List of figures **Page**

List of tables

Page

CHAPTER 1

1 INTRODUCTION

1.1 STUDY AREA

The Magadi area is in the southern part of the Gregory Rift Valley which itself is part of the East African Rift system. The Gregory Rift is of the continental rift type (Gregory, 1921); it extends from Magadi-Natron basin in the south to Baringo and Suguta grabens in the north and is a complex graben bisecting the Kenya domal uplift. The southern Kenya Rift is the youngest portion of the rift system commencing with late miocene volcanism and faulting (Baker, 1958; Crossley and Knight, 1981). The present day rift situation in the southern Kenya Rift is characterized by a narrow rift width of 50-70 km. The shoulder rift elevations are about 4000 m and 2000 m respectively. The volcanics and sediments reach a thickness of about 3500 m-4000 m whereas from the shoulders, they reach a maximum thickness of about 1500 m (Chapman *et al.*,1978; Swain *et al.*,1981; Henry *et al.*,1990).

Lake Magadi is located in a broad flat depression that occurs at the lowest point in the southern Kenya Rift Valley. Hydrogeological studies indicate that this is the point to which all ground water flow in the southern rift is directed (Clarke *et al*, 1990). Hot springs are also distributed along the shores of Lake Magadi as shown on the location map of the study area in figure 1.1. These hot springs which number over 200, issue from the base of the fault scarps bounding the lake. The hottest springs (80°-95°C) are located on the northern end of the lake with the rest of the lakeshore springs recording warm

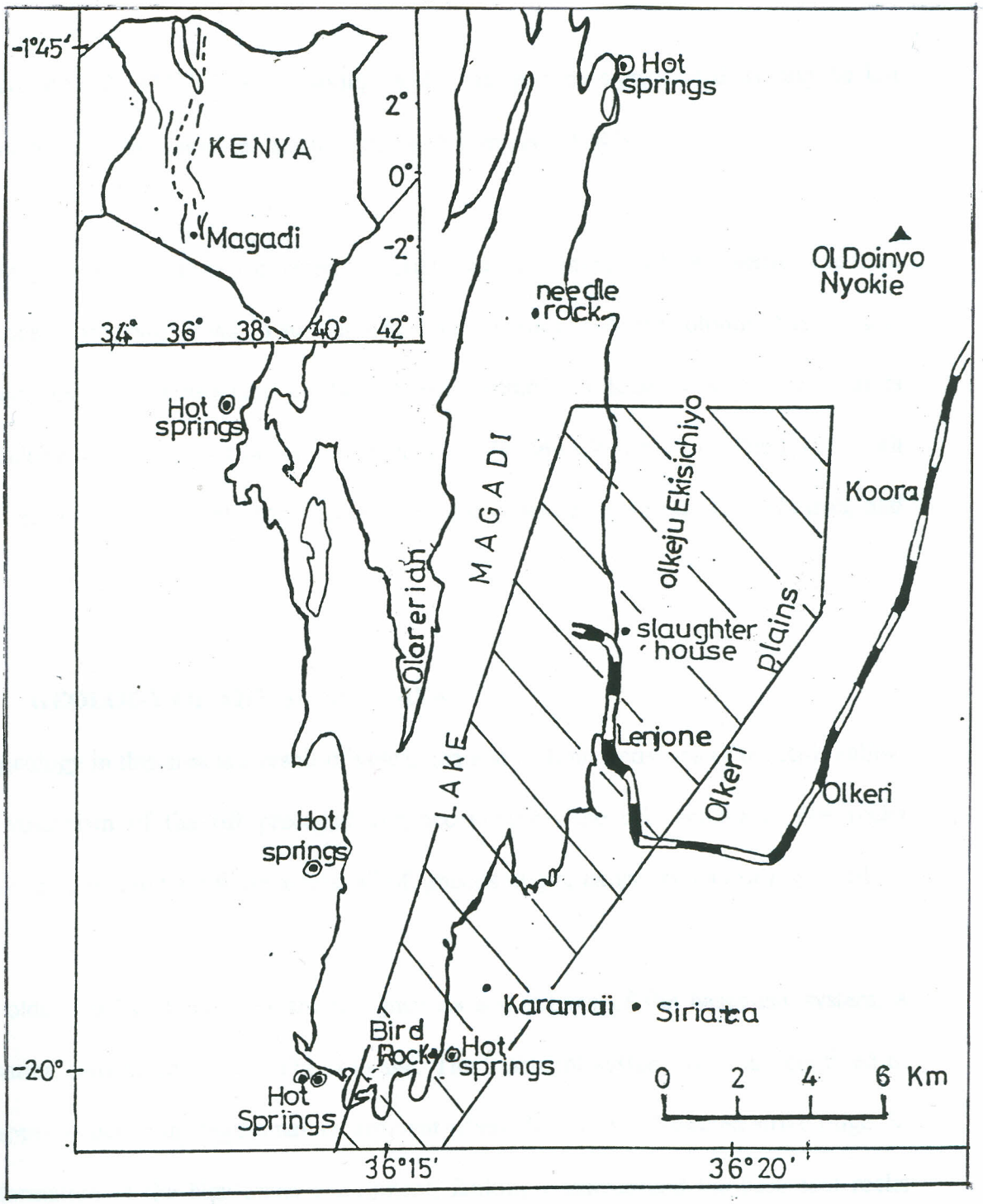

LEGEND

Railway

Study area

Hot springs

Figure 1.1 Location Map of the Study area

temperature (32°-44°C). The hot springs and steam jets are signs that there may be hot magma not very far below the earth's surface (Nyamweru, 1980).

The Magadi area is largely covered by Quaternary sediments, which overlie extensive pleistocene trachyte lavas. The trachyte lava overlies pliocene olivine basalts and nephelinites which in turn rests on the Archean basement. A dense network of grid faults that belong to the rift floor faults affects the area. These faults especially the north-south trending fault scarps, control the occurrence of geothermal manifestations. (Riaroh, and Okoth, 1994).

1.2 GEOLOGY OF THE STUDY AREA

The geology in this area is a result of volcanism and tectonic activities of the Rift Valley. The volcanism of the rift preceded and accompanied the rift tectonism. The rocks outcropping within the rift are almost all of igneous origin, either primary or reworked.

The oldest rocks in the area are the gneisses and schists of the basement system, a formation considered to be Archean in age. The basement system rocks are confined to the upper slopes of the Nguruman escarpment where they form a dissected strike ridge. In the formation of the Nguruman escarpment, faulting occurred and the basement rocks were down thrown to the east followed by erosion. A series of olivine basalt lava (Kirikiti basalts) erupted on the down thrown side of the fault, and inundated the lower side of the escarpment (Baker, 1958).

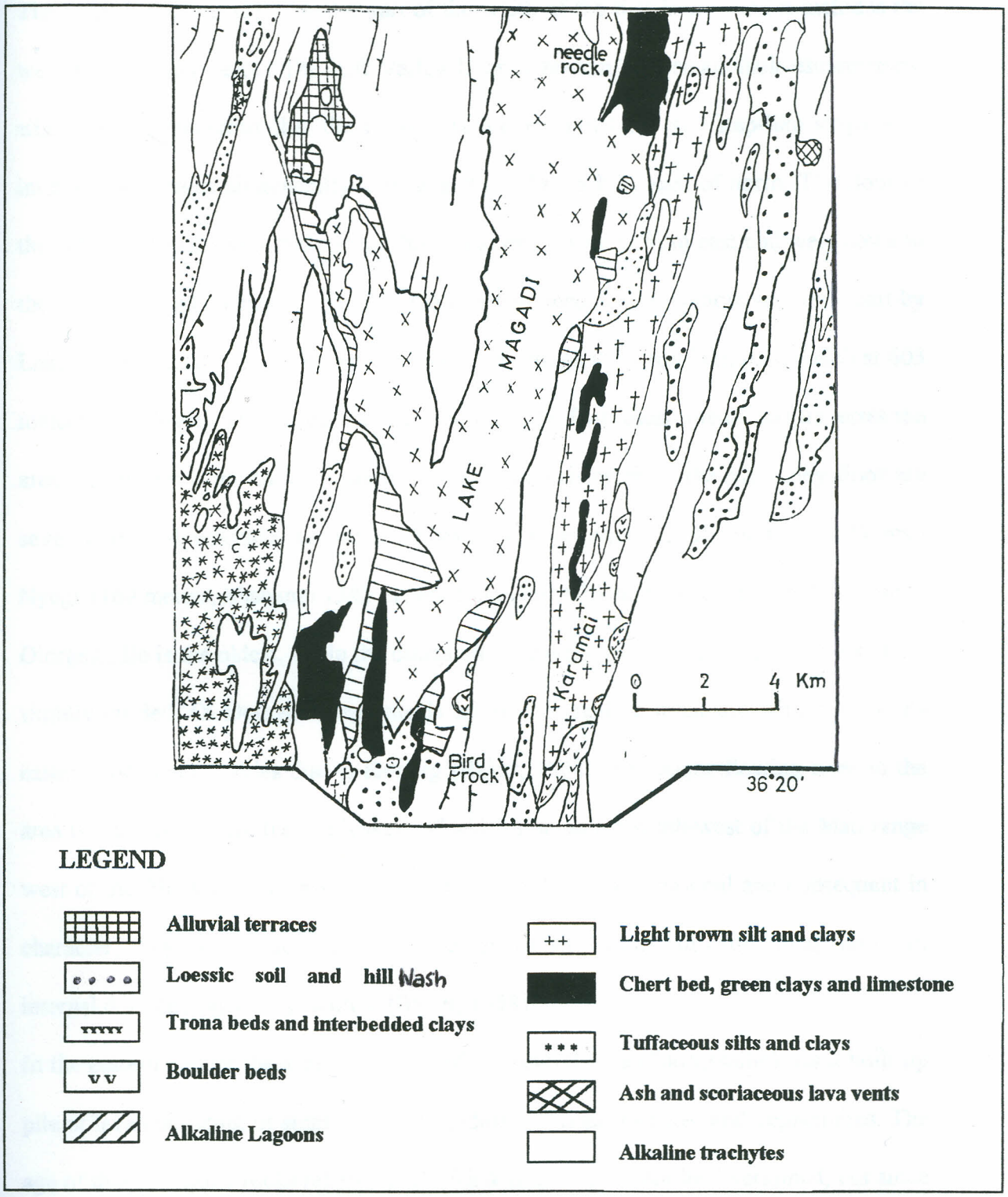

Figure 1.2 Geological Map of the study area (after Baker, 1958)

The Magadi area covers a greater part of the width of the Rift Valley and it includes the western boundary faults. The Rift Valley floor is broken into small fault escarpments, which are so numerous that the country is broken into table and step-like strips with intervening troughs all generally narrow and trending a little east of north. The floor of the valley descends with many steps due to the escarpments, from east and west down to the deepest trough, which is central in the area and occupied in its more southerly part by Lake Magadi. Lake Magadi occupies the Magadi trough in its southern part, which at 603 meters is the lowest part in this area. It is bounded by fault escarpments and traverses the area completely from north to south. In this region rising from the rift valley floor are several isolated volcanic mountains. These are Olorgesailie 1762 meters, Ol Doinyo Nyegi 1169 meters, Shanamu 1341 meters and minor hills such as Kisamis and Koriamat. Olorgeisailie is the oldest, while the others are relatively young in geological age and are slightly eroded. Ol Doinyo Nyegi stands up as a dome-like mountain with cliff on its eastern and western sides due to faulting (Baker, 1958). The major flowing river in the area is the Uaso Nyiro, the headwaters of which rise on the south-west of the Mau range west of the Rift Valley. Streams on the grid-faulted area are seasonal and consequent in character; they flow either into Lake Magadi or into small alluvium filled basins of internal drainage caused by faulting (Baker, 1958).

In the eastern part of the area, a volcano of the central type (Olorgesailie) has a built up pile of lava consisting of augitites, trachyandesites, alkali trachytes and nephelinites. The age of these volcanic rocks relative to the Kirikiti basalts cannot be determined, but since olivine basalts similar to Kirikiti basalts occur resting on Olorgesailie lava, the Kirikiti basalts are tentatively correlated with them and thus appear younger as the Olorgesailie

lavas in the table of geological succession. There is evidence that the faulting on the eastern side of the rift valley did not begin until after the Olorgesailie volcanicity, for nephelinites similar to those forming the upper part of the Olorgesailie have been found in the upper part of the escarpment between Singaraini and Ngong. Resting on the plateau trachyte in the north of the area is the orthophyre-trachyte, a distinctive rock closely allied to the plateau trachytes in composition but differing greatly in appearance and mode of weathering. The plateau trachyte volcanicity was brought to a close by the formation of a number of small ash and scoriaceous lava cones, all small with the exception of Ol Doinyo Nyegi. On the almost level surface of alkali trachytes, a thin layer of lake beds (Oloronga beds) consisting mainly of reworked volcanic dust and debris was deposited (Baker, 1958). This is illustrated in the geological map of the study area figure 1.2.

Grid faulting which is so easily seen at the present day followed the deposition of the Oloronga beds. Numerous sub-parallel faults cut the rift valley floor at that time resulting in down faulting of the central part, which is now occupied by Lake Magadi. Several subsidiary fault troughs were formed and lake sediments accumulated in them. The Olorgesailie lake beds, which contain Acheulian artifacts and fossils of middle pleistocene age, accumulated as diatomaceous clays, while in the Uaso-Nyiro depression fine silts and clays accumulated (Baker, 1958). Cherty rocks consisting largely of silicified-bedded clays were laid down in the Magadi fault-trough although deposition of these beds might have began before the grid faulting ended. A further period of lake deposition was confined mainly to the Magadi trough and the Uaso-Nyiro basin.

Elsewhere lacustrine gravels and clays were deposited in fault troughs. In the Magadi trough, fine silts and clays (high Magadi beds) were laid down to a level 12.2 metres higher than the present surface of the lake. Later these beds were partly eroded from the trough, mainly by wind action. Finally the onset of alkaline spring activity, together with accumulation of mud during wetter periods, resulted in deposition of a series of beds of sodium carbonates intercalated with clays. These form the evaporite series which is still in process of formation at the present day (Baker, 1958). The table 1.1 illustrates geological succession in Magadi area.

1.3 STRUCTURE

The southern segment of the rift becomes progressively more north-south in orientation further south when passing the central trough. In Magadi area, the structural elements of geology are clearly recognizable. This is due to the short geological history of most of the rocks, which apart from the basement rocks range from tertiary to recent in age. Features of tectonic origin have less been affected by erosion since faulting is the dominant factor in the structure, it determines not only geological lines but also the topography (Baker, 1958).

Table 1.1: Table of geological succession in Magadi area

Recent	Evaporite series	Boulder beds
	Erosion	
Upper pleistocene	High Magadi beds	Uaso-Nyiro alluvium
	Minor faulting and Erosion	
Middle pleistocene	Olorgesailie lake beds Chert series	Ngare Nyiro beds
	Grid faulting and Erosion	
	Oloronga beds	
	Minor volcanic vents	Ol Doiyo Nyegi volcanics
	Orthophyre trachyte	
Lower pleistocene	Plateau alkali trachytes	
	Rift faulting Second Nguruman fault	
	Lengitoto trachyte and underlying sediments	
Pliocene	Olkeju Nero basalts	Kirikiti basalts
	Olorgesailie volcanics	
	First Nguruman fault	**Erosion**
	Erosion	
Archean	Basement system	

(After Baker, 1958)

The main structural features of the southern segment are N160° major faults and a network of north- south to N 10° small faults in the Magadi trough. The N160° faults cut the north-south and N10°E faults. These dominant faults occur on both the margins and in the rift, and include the Naitami, Endosapia, Lengitoto and the west lake Magadi faults and the western fault border of the Ngong volcano as illustrated in figure 1.3. The Magadi trough is asymmetrical, bordered to the west by a narrow fault zone that exhibits significant vertical movements (Lengitoto, Nguruman escarpment) and to the east by a large, faulted flexure consisting of a broad zone of numerous faults each with minor down throw that spreads over half of the trough. The inner trough is crossed by numerous minor faults separating blocks between which are exposed small elongate basins occupied by quaternary detrital sediments (Baker, 1963). The N10° trending Nguruman faulted escarpment represents the western border of the rift in this area formed northward by the Lengitoto fault. The large vertical displaced of the fault forms an escarpment 1400 m between the lip of the rift, at 200 m above the sea level (a.s.l.), and the valley floor at 600 m a.s.l. Faults along this escarpment have probably been active since the rift system was initiated in the miocene. The cumulative vertical movements are estimated to be between 1200-1500 m (Baker, 1963). Right-lateral movements along this fault are reported (Vidal, 1985) and are attributed to the miocene rifting episode.

The Lengitoto fault is one of the major faults trending in a N160° direction and sharply cuts the Lengitoto precambrian anticline. This fault is likely to have been active in early miocene time, left lateral movements along it are attributed to early miocene rifting, in response to the extension that is inferred to have been directed N170° to north-south

(Vidal, 1985). Based in structural observations in lower Miocene volcanic rocks, (Vidal, 1985) inferred an episode of early to middle Miocene extension directed N170° to north-south associated with initial rifting. He observed evidence for this stress in the Lengitoto, Mau and Elgeyo fault areas on the western margin of the rift and the Sattima fault in the Aberdare escarpment. The grid faults, which occur across the whole width of the rift valley, cut the level surface formed by plateau trachytes. The bulk pile of lava on Olorgesailie mountain has effectively stiffened the crust on which it rests and to the south of the mountain extends a strip of lavas that has been prevented from faulting.

1.4 LITERATURE REVIEW

In East African Rift Valley separation is taking place within the continental lithosphere. The continued spreading of this rift will probably split the African continent and produce new ocean floor. The driving mechanism for plate motion is connected with convective movements in the mantle, the internal heat of the earth being the source of energy. Abnormal terrestrial heat flow occurs along the spreading and converging plate boundaries. The mass transfer of heat by magmas generated from the mantle carries heat to the shallower levels of the crust. From such heat sources, geothermal systems develop. All prospective high enthalpy geothermal regions of the planet therefore are found within belts of geologically young volcanism and crustal deformation produced by lithospheric plates in motion (Bowen, 1979).

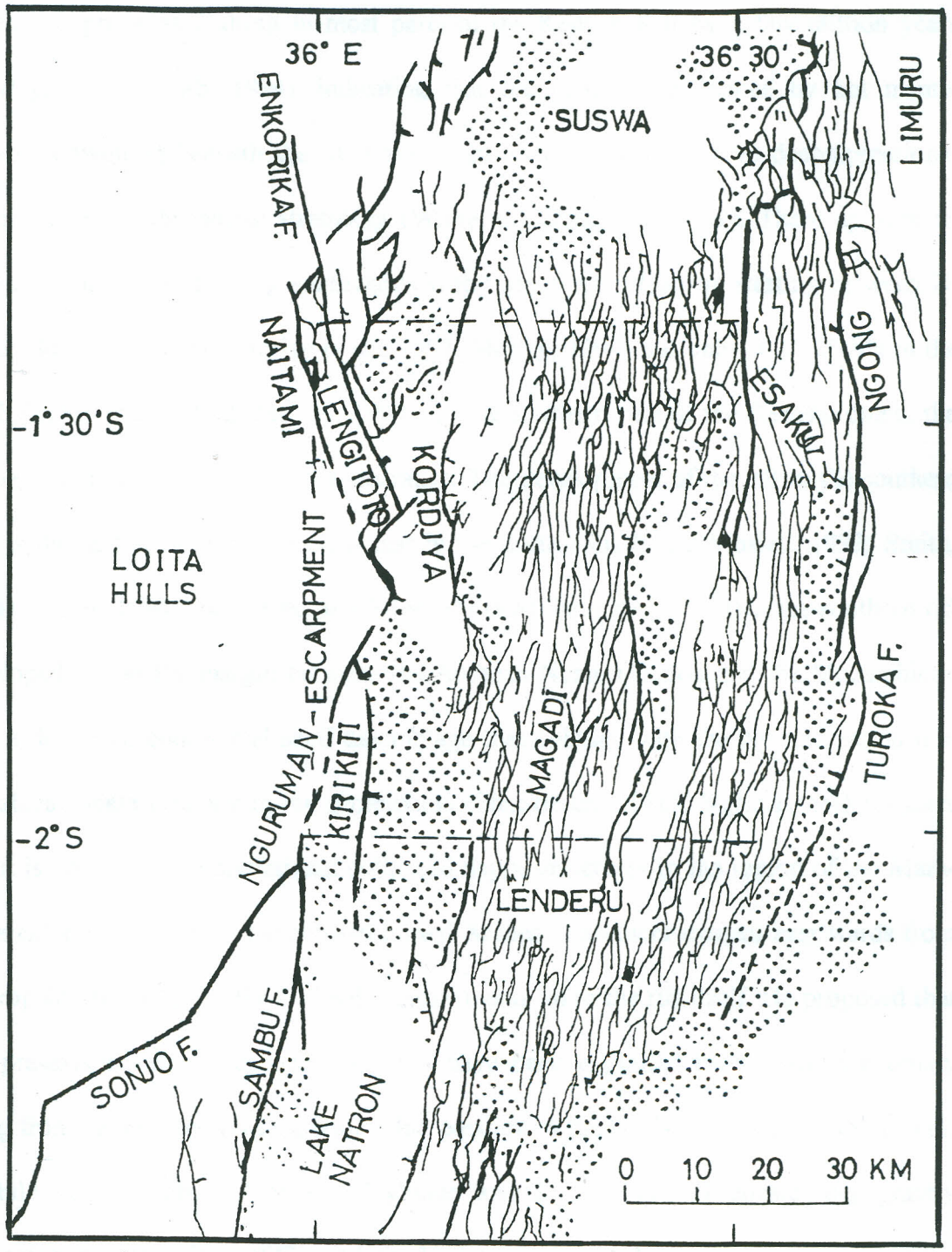

Fig. 1.3 Structural map of the study area.

Volcanism precedes faulting in most parts of the Kenyan Rift by a few million years (Morley, 1994; Smith, 1994), indicating that the melts were formed by hot mantle material upwelling beneath the rift rather than in response to passive decompressional melting due to lithospheric stretching (White and Makenzie, 1989). There appears an overall propagation of rifting southwards with time, with volcanism starting between 28 and 33 Ma in the north (Morley *et al.*, 1992; Morley, 1994) but only 16 to 20 Ma in the south (Baker *et al.*, 1972; Morley, 1994). In the southern part of the Kenyan dome, the rift begins to lose its graben-like appearance. The development of the rift in the southern area is thought to be different from that in the north (Smith and Mosley, 1993; Smith, 1994). Smith (1994) and Hetzel and Strecker (1994) have proposed that the southern rift developed across the margin between the Archean Nyanza craton and the Mozambique belt, a deformed continental shelf assemblage that collided with the Nyanza craton in a Himalayan scale orogeny in the proterozoic (Shackleton, 1986). Smith (1994) suggests that it is obscured by gravitational collapsed nappe structures in the region of the Mara-Loita Hills to the West of the rift and buried Archean basement extends east wards from outcropping boundary at the Oloololo escarpments up to the rift itself. He proposed that this pre-existing structural weakness may have been exploited by a thermal anomaly rising from beneath the Nyanza craton and position of the rift is controlled by the Craton -Mobile belt boundary. However Nyblade and Pollack (1992) considering gravity transects across the rift at different latitudes have interpreted the gravity anomaly in the southern part of the rift as due to a rift component (a shallow rift basin, lower crustal intrusion and low density upper mantle) and a 'suture' component arising from a crustal root beneath the Nyanza Craton and Mozambique belt boundary. Below the southern

part of the Kenya rift, Mechie *et al.* (1996) estimated from KRISP 1990 (Kenya Rift International Seismic Project) data that the onset of melting at a depth of 50 ± 10 km, on the basis of anomalously low velocities interpreted to be caused by partial melt. Also for the southern Kenya Rift, seismic P-wave velocity information shows that the crust-mantle boundary outside the rift occurs at about 42 km depth (Bonjer *et al.*, 1970; Maguire and Long, 1976).

The variations of Bouguer anomaly over the East African rift includes two minima and a short wavelength maxima (Beicip, 1987). These features are interpreted as caused by summation of a negative anomaly due to local culmination of the asthenosphere penetrating high density upper mantle and lower crust and of a positive anomaly due to intrusions within the upper crust. This is supported by a specific gravity survey in the Kenya Rift (Baker and Wohlenberg, 1971). Beneath the rift, the crust mantle boundary occurs at about 35 km depth (KRISP working group, 1987; Henry *et al.*, 1990). Thus the crust-mantle boundary uplift is 5-7 km. Additionally, a zone of low P-wave velocities (7.5 - 7.7 km/s) below the rift has been detected whereas outside the rift, P-wave velocities appear to be normal (8.0 - 8.1 km/s). (Bonjer *et al.*, 1970; Maguire and Long, 1976). This deduces the presence of partial melt in the low velocity zone of the mantle beneath the rift.

From magnetotelluric investigations of the rift carried out by Banks and Ottey (1974), Rooney and Hutton (1977), Banks and Beamish (1979), regions of anomalously high conductivity beneath the Rift were identified. They considered this as evidence for

presence of partial melt beneath the rift. They estimated the amount of partial melt beneath the rift at less than 5 percent which was in good agreement with modern estimates of 3 to 5 percent partial melt (Mechie *et al.* 1994). From an LMT (Long period Magnetotelluric survey) (Simpson *et al.*, 1997) in the southern part of the Kenyan rift, the Nguruman fault was clearly detected in addition to enhanced conductivities, increasing to the north below the Rift graben itself. Crustal thinning at lake Magadi about 100 Km south of the Kenya dome is less than that at lake Baringo about 100 Km north of the dome. In addition, the Magadi section of the rift valley is flanked by considerably thicker crust to the east (38-44 Km) than the west (< 35). The major Nguruman fault bounds the rift valley on the west near lake Magadi. (KRISP WORKING GROUP, 1995).

Heat flow in Kenya is high but variable. There is spatial association among high heat flow and quaternary volcanism, faulting and hydrothermal manifestations, strongly suggesting that high heat flow is ultimately magmatic in origin redistributed in the shallow crust by hydrothermal activity. This is supported by specific studies of the geothermal fields in the Kenya Rift (Riaroh and Okoth, 1994). Williamson (1975) showed that the Kenya Rift axial high heat flow anomalies can in part be modelled with young dyke intrusions into the axis of the rift. The existence of such intrusions was predicted from gravity data (Baker and Wohlenberg, 1971). Healy (1975) explained that the source of heat in such a system is to be related to the concentration of intrusive dikes arising from an intra-crustal magma reservoir. He further noted that this vigorous activity has caused acidic magma to rise close to the surface. Numerous hot springs are distributed on the shores of lake Magadi. Hot springs often with temperatures near 100°C

are common surface manifestation of high temperature geothermal systems. Chemical analysis generally indicates that the water from such springs is meteoric in origin, implying that the hot springs results from circulating ground water which extract heat from high temperature subsurface rocks (Waring *et al*, 1965). The driving mechanism of hot springs in geothermal areas is a combination of pure hydrostatic pressure and differential pressures due to thermal expansion of the water. Warm or thermal springs with temperatures of a few tens of degrees above the mean air temperature are believed to be caused by downward circulation and heating by the normal geothermal gradient. A suitable geological structure allows the water to return to the surface as a spring. Springs on land are usually found in fault and fracture zones (Waring *et al*, 1965).

Two aeromagnetic surveys have been carried out in Magadi area. The Magadi and Hannington surveys were sponsored by UNESCO (Wohlenberg and Bhatt, 1972). The purpose of this work was to find out, whether it was possible to detect by magnetic method the tops of intrusive bodies beneath the extensive lava flows that cover most parts of the rift floor. In the lake Magadi aeromagnetic survey, an area of 3750 km^2 and 865 line kilometres were flown. Strong anomalies were observed on the eastern border of the survey, near Olorgesailie volcano and on the north near Suswa volcano. Most of the linear features detected trend NW-SE. The more intense anomalies correlated with exposures of volcanic rocks that have much stronger magnetic susceptibility than other lava of the area. A more comprehensive analysis of the lake Magadi aeromagnetic survey data was done by Wolff (1992) from which several anomalies were detected at the near

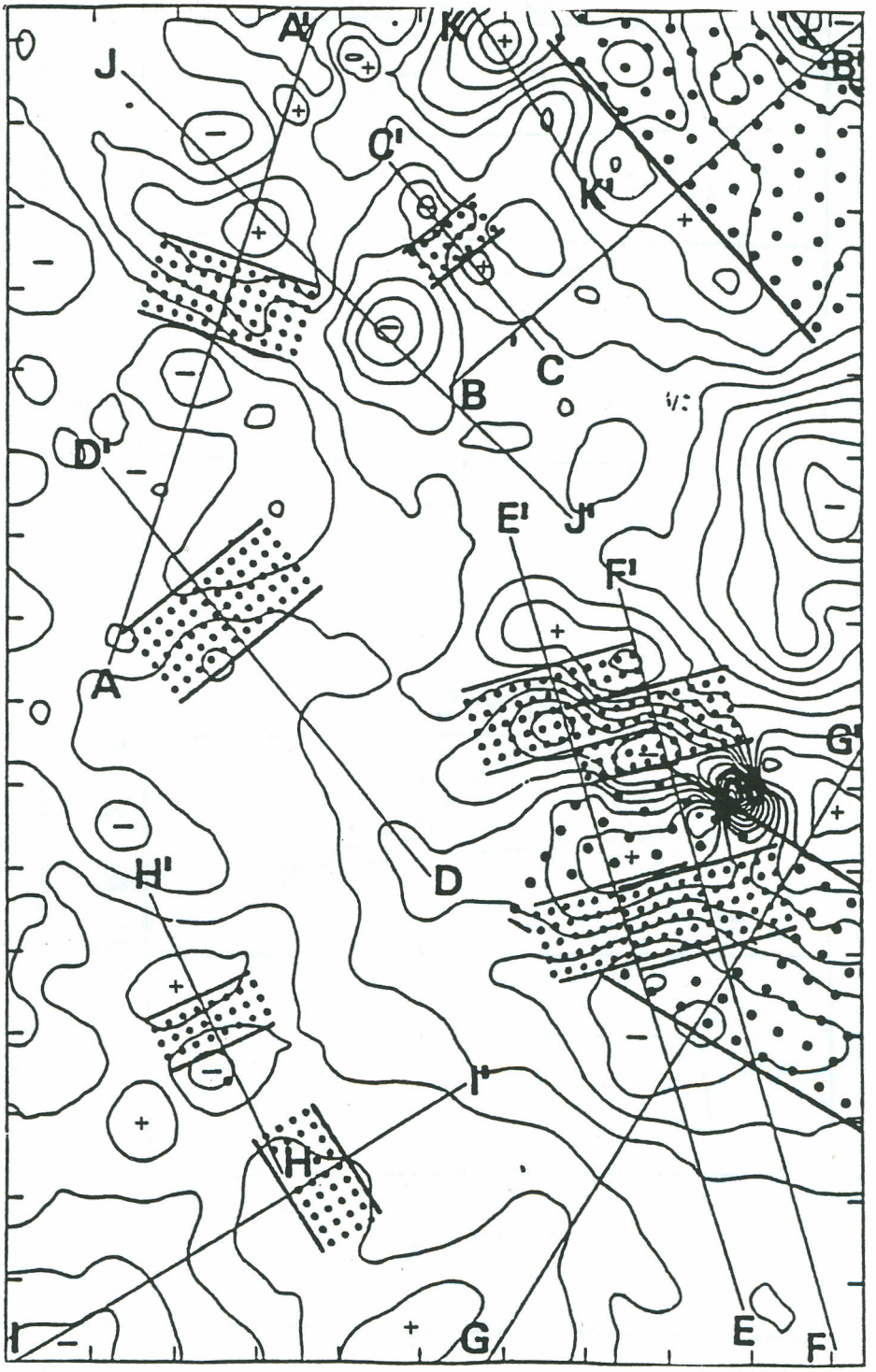

Fig. 1.4a Total Magneticfield anomaly map showing profiles and anomalous bodies (after Wolff, 1992)

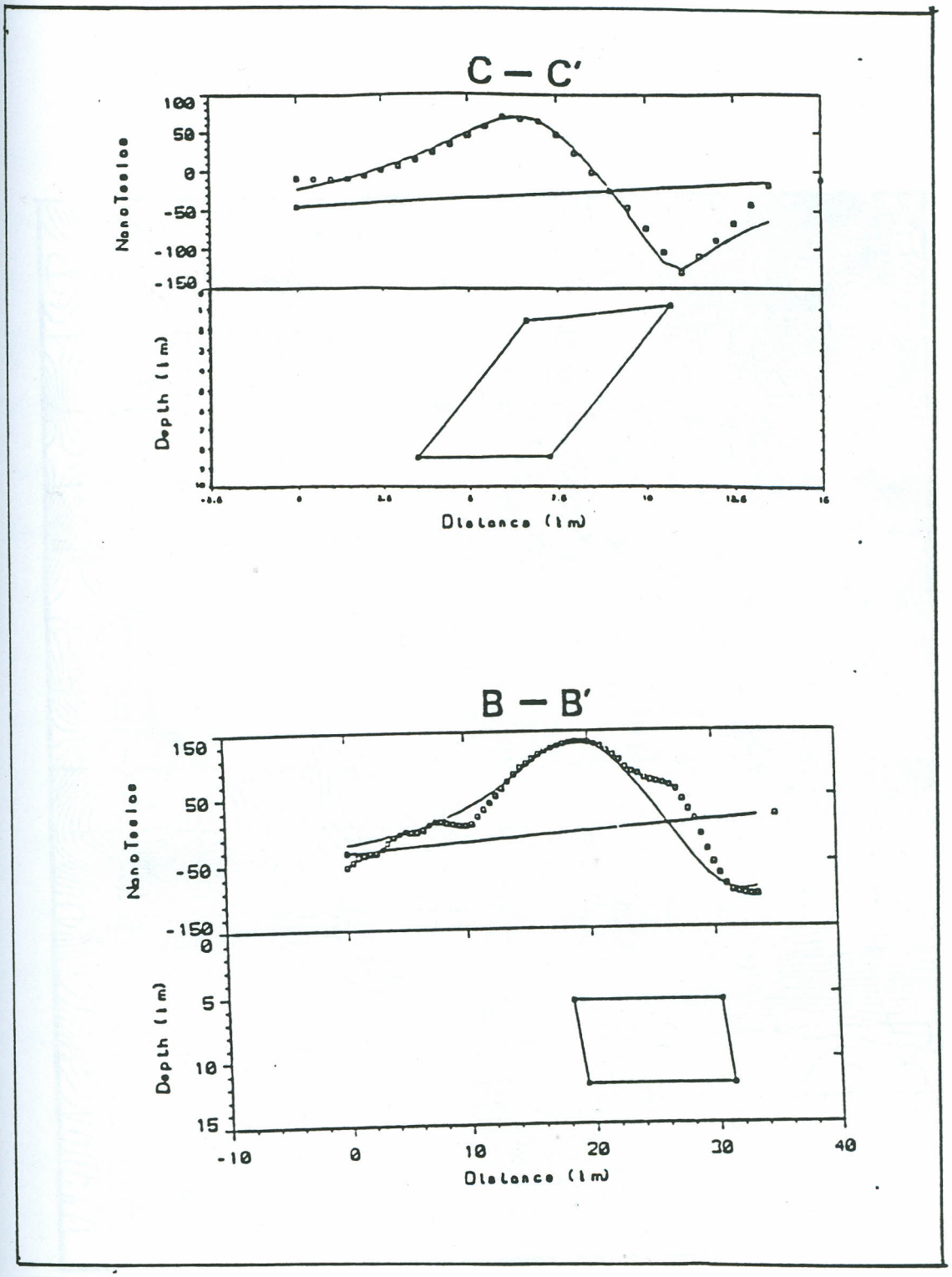

Fig. 1.4b Anomalous bodies in profiles B–B^{1} and C–C1 (after Wolff, 1992)

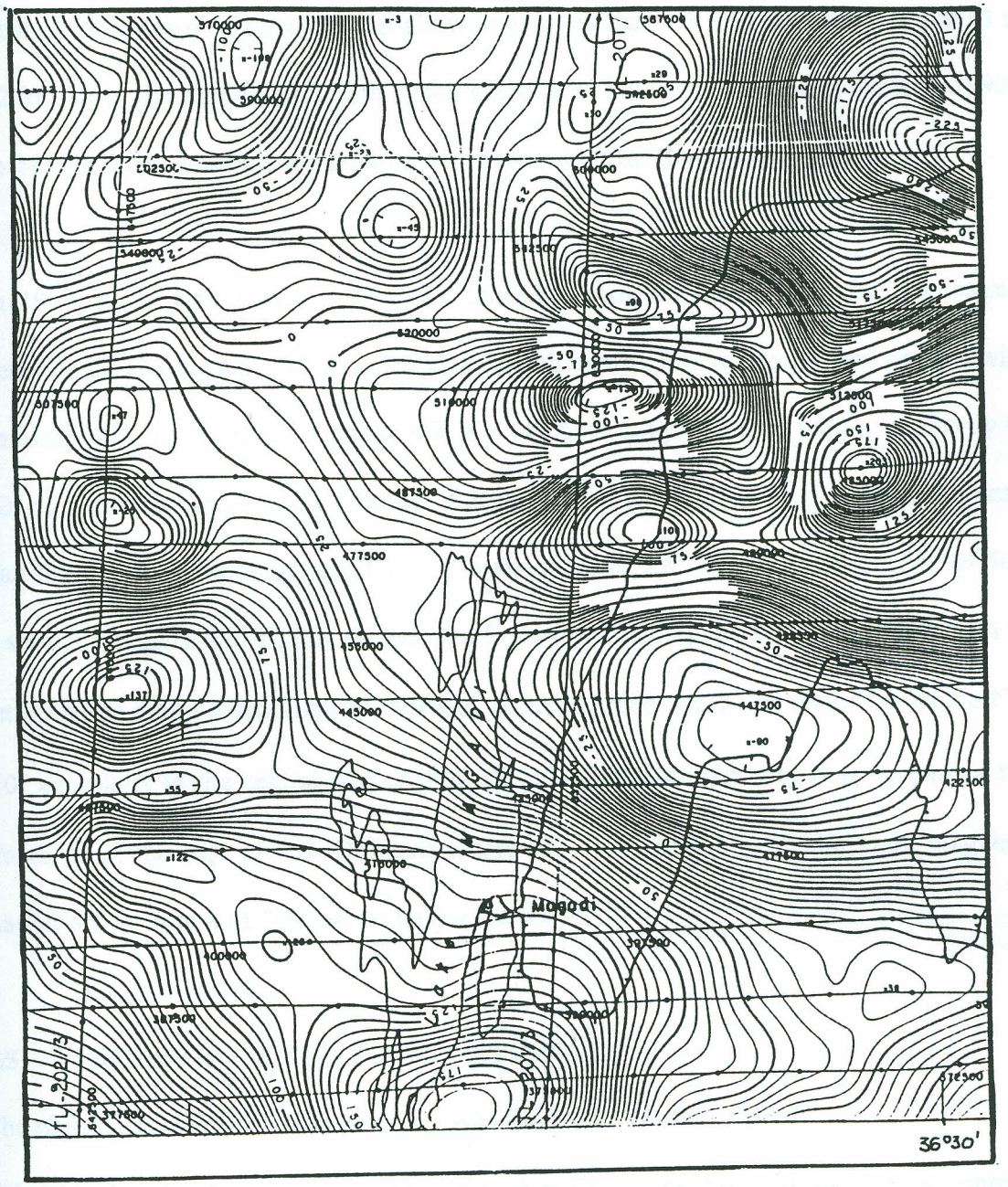

Fig. 1.5. Aeromagnetic map of the study area (after CGG, 1987)

Nguruman and north-west to the study area at Olorgesailie as illustrated in figure 1.4(a). Most of these were interpreted as shallow anomalies figure 1.4(b) occurring at depths of 1-2 km from the surface and with depth extends of between 3.5-15 km (Wolff, 1992). These anomalies detected are situated out of the area considered in this work.

In 1987, an aeromagnetic survey was carried out on the tertiary rift by Compagnie Generale de Geophysique (CGG, 1987) a French exploration company on contract with National Oil Corporation of Kenya (NOCK). A varian magnetometer with a sensitivity of 0.01nT was used and a flight altitude of 2896 meters was maintained. An aeromagnetic map from this survey constructed with a scale of 1:250,000 with contour interval of 5nT is shown in figure 1.5. In this survey, the Suswa volcano appears as a magnetic high in between two major discontinuities oriented N 30°. Further south, the major trends are N 5 -10° especially in the central part of the rift, the Magadi trough. The deepest part of the graben is in the east of Lake Magadi where the depth estimates to the main magnetic marker are in excess of 200 metres below the sea level.

1.5 THESIS OBJECTIVES AND RATIONALE

The objectives of the research project are as follows:

(a) to detect zones or bodies at depth with sufficient magnetic susceptibility contrast that may indicate presence of intrusive dykes. Certain parameters like depth, depth extent, dip angle, strike direction and their width will be determined for found bodies.

(b) to establish whether the detected bodies are the causes of the hot springs which could be potential geothermal reservoirs.

Geophysical signatures over modern rifts strongly suggests that the rifts are associated with crust that departs significantly in character from a standard continental crust. The results of seismic, gravity and aeromagnetic surveys indicate that modern rifts are commonly underlain by relatively thin crust and lithosphere, and by an upper mantle that contains an anomalously low density asthenosphere diapir (Beicip,1987). The Kenya Rift Valley, a part of the East African Rift Systems, like other rift systems, characterised by an anomalously low gravity in the graben proper, caused by updoming of less dense asthenospheric material, producing a lithospheric thinning. Within the graben axis, small local gravity highs are superimposed on the generally low gravity values. They are very likely caused by magmatic intrusions in the crust. Local gravity anomalies in a geological environment associated with young volcanism and tectonism are usually indicative of geothermal conditions at the intermediate depths (Ndombi ,1978).

Local gravity highs were mapped in Magadi in the Kenya Tertiary Rift study, an exploration promotion project assisted by World Bank (Beicip,1987). Thus there was a need for a follow up survey to establish the possible sources of the gravity highs and whether they can be potential heat sources for geothermal energy. A ground magnetic survey was carried out to map any local magnetic anomaly related to the axial gravity highs observed in the region. With the view that the intensity of magnetization can only

exist below Curie point temperature, a hot body with a temperature above Curie point would not produce any magnetic signature.

Stations were established with a separation of about 1 km. The raw magnetic data were reduced by correcting for both the diurnal and geomagnetic variations. From the reduced data, contour maps were prepared and from them, qualitative interpretation was attempted. This involved defining regions of magnetic anomalies in the subsurface. Quantitative interpretation was also carried out which involves fitting the observed data to a model along the selected profiles. The geology of the area and previous geophysical studies in the area were used as controls to the final models.

CHAPTER 2

2 MAGNETIC SURVEYING

2.1 INTRODUCTION

The magnetic geophysical prospecting method which involves mapping the earth's magnetic field is important in guiding our speculation on the portion of the earth's subsurface containing bodies with appreciable amount of ferromagnetic minerals. Rocks and ores containing magnetic minerals become magnetized by induction in the earth's magnetic field. Magnetic exploration thus involves mapping variations in the magnetic field to determine location, size and shape of the causative bodies. Whereas the earth's normal magnetic field is more uniform over areas of homogeneous magnetic material, it is locally distorted where concentration of rock material of high magnetic susceptibility are present e.g iron minerals such as ilmenite and magnetite. Since crystalline rocks contain much higher proportions of these minerals than do normal sediments, the magnetic anomalies which result from the presence of intrusions of basic or even ultrabasic material may show existence of arching and structural traps in the overlying sediments. Determination of depth to the basement with the magnetic method may serve as a measure of thickness of sedimentary section present (Hobson and Tiratsoo, 1985).

Rocks of igneous origin are known to be magnetic and therefore affect the geomagnetic field. The magnetic method hence can be used in delineating intra-sedimentary magnetic sources such as shallow volcanics or intrusives that perturb the normal sedimentary sequence. Sedimentary rocks produce a negligible magnetic effect compared with igneous rocks, such that most variation in magnetic intensity measured at the surface

result from topographic or lithologic changes associated with the basement or from igneous intrusives. Magnetic materials are known to lose their magnetization when their temperature reaches the Curie point temperature. Conversely, melted rocks acquire their magnetization when they cool below the Curie point. For magnetite which is the most common magnetic material, the Curie point temperature is about +580°C. Due to the earth's internal heat, magnetic rock properties can exist only at temperatures cooler than the Curie point which limits the sources of magnetic anomalies to a maximum depth of 30-40 km. In areas of high geothermal gradient, the Curie point temperature may be reached at relatively shallow depth which means that below this depth, the rocks cease to be ferromagnetic. In such areas, the basement rock would not have any magnetic expression since it occurs below the Curie point depth. The magnetic method hence depends on measuring accurately anomalies of the geomagnetic field which occur above the Curie point depth produced by variation in intensity of magnetization in rock formations.

2.2 CHOICE OF THE EXPLORATION METHOD

Different geophysical techniques may be used in the search for a hot body in the subsurface, which might be a potential source of geothermal energy. The magnetic method as an exploration tool can be used in limited or regional scale. The former is concerned with ground magnetics while the latter is solely concerned with aeromagnetics. Regardless of scale, the prime objective of choosing a method is to secure maximum information at minimum cost and to provide service which is but part of an overall exploration sequence (Ward, 1958; Riley, 1959). As well, the choice of the method will

depend on expected depth of occurence, the geometry of typical occurences in any given district etc. The patterns, which seem to offer the most advantages, must be developed. Magnetic surveys have their most obvious and economically important application in the exploration of new areas. Rapid and relatively inexpensive airborne magnetics can determine the depth to the basement quite reliably to a precision of the order of 5 percent or less of the depth below the flight level (Nettleton, 1976). Land surveys are slow but can be positioned with great accuracy and are used for detailed follow-up of areas identified as interesting in airborne reconnaissance surveys.

The magnetic method was considered the most appropriate geophysical technique in this work due to the fact that the bottom to the magnetic bodies can be detected which may indicate the Curie point depth. This method was considered cheap and sensitive in measuring a magnetic body to any depth.

2.3 THEORY OF MAGNETIC METHOD

2.3.1 Elements of the earth's magnetic field

The geomagnetic field, like any magnetic field is a vector field. At any point on the earth's surface it is represented by a vector pointing in the direction of force on a positive pole, and having a length proportional to the strength of the field at that point. Its components are called magnetic elements. Among the magnetic elements, the direction of the field is the element least sensitive to changes in the dimensions and magnetic properties of the subsurface body. The various magnetic elements are B_Z, B_H, B_T, D and I which describe the earth's magnetic field. These elements are represented in the parallelepiped in figure 2.1. The angle between the magnetic and geographic meridians is

the magnetic declination D while that between the total geomagnetic field vector and the horizontal plane is the magnetic inclination I. These geomagnetic elements vary all over the earth's surface. The line where inclination I is zero is the magnetic equator and points where the inclination is +90° and -90° are the north and south magnetic poles respectively.

The total field vector B has a vertical component Z and a horizontal component H in the direction of the magnetic north. The vertical component Z is positive north of the magnetic equator and negative south of it (Parasnis, 1986). The dip of B is the inclination I of the field. B varies in strength from about 25,000 nT in equatorial regions to about 70,000 nT at the magnetic poles.

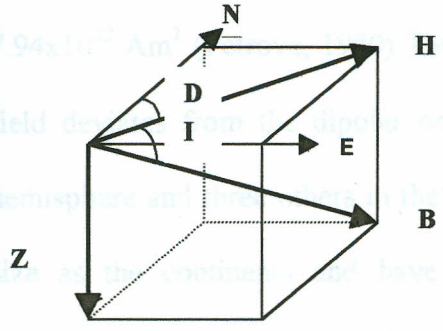

B = Total intensity vector
Z = Vertical component of the geomagnetic field
H =Horizontal component of the geomagnetic field
D= Angle of declination
I= Angle of inclination
E= Geographic East
N= Geographic North

Figure 2.1 Geomagnetic Elements

The elements of the magnetic vectors as in figure 2.1 are related as by below equations:

$$B = H/\cos I \quad (2.1)$$

$$B^2 = H^2 + Z^2 \quad (2.2)$$

$$B = H \tan I \quad (2.3)$$

2.3.2 The geomagnetic field

This is the magnetic field of the earth, which can be measured at any part on the earth's surface. The magnetic field on the earth at a given place and time may be considered to consist of three parts. These are the main field which is slowly changing, a diurnal part that changes with time which is approximately repeated in daily cycles and the anomaly part caused by inhomogeneities of the earth's crust.

The main field is the undisturbed component of the earth's field which to the first approximation can be mathematically represented as a dipole field. The best fitting dipole has its axis inclined at 11.5° to the earth's rotation axis, and its centre is displaced about 400 km away from the geometric centre of the earth towards the south-western pacific (Petrova, 1980), the displacement reflecting the asymmetry of the magnetic field on the earth's surface as illustrated in figure2.2. The dipole moment is approximated as 7.94×10^{22} Am^2 (Petrova, 1980) There are areas over the earth's surface where the actual field deviates from the dipolar one. Three of these areas are located in the northern hemisphere and three others in the southern hemisphere. These areas are about the same size as the continents and have been called continental or world anomalies. The geomagnetic field undergoes slow changes in intensity and direction with periods from 20 up to 8,000 years called the secular variation. There also exists a westward drift of the magnetic field, to the first approximation contours of the continental anomalies and the phase of the secular variation are drifting westward at a rate of 0.2°/ yr (Petrova, 1980).

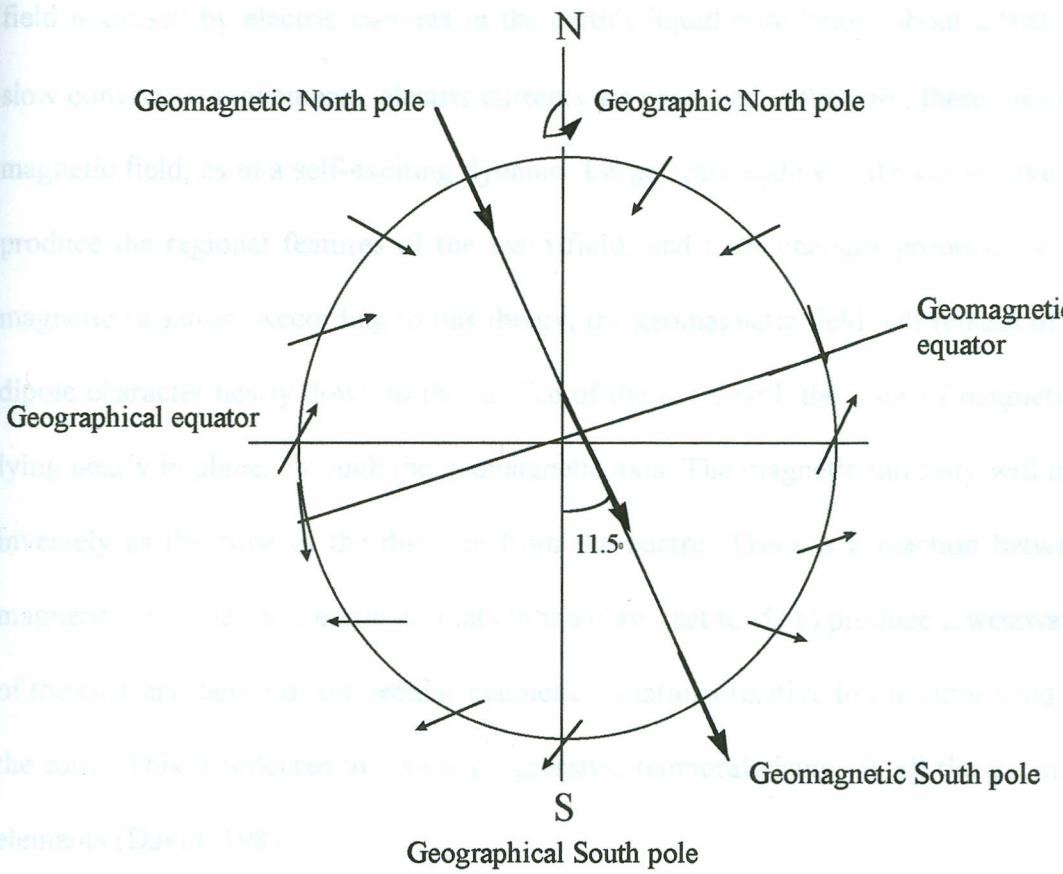

Figure 2.2 The earth's dipole field (after Militzer & Weber,1984).

According to paleomagnetic studies, from time to time reversals of the magnetic polarity occur, in which magnetic poles swap places. Such reversals have occurred rather frequently in the history of the geomagnetic field, the frequency being different during different geological periods. There were epochs when reversals followed after intervals of 10^5 years; at other times, the field kept its polarity for a span of tens of million of years (Petrova, 1980).

The origin of the main field and its secular variation is the earth's core according to accepted theories by (Elasser, 1956) and (Bullard, 1949). It seems probable that the main

field is caused by electric currents in the earth's liquid core below about 2,900 km. By slow convective movements, electric currents are produced in the core; these maintain the magnetic field, as in a self-exciting dynamo. Large scale eddies in the convective motion produce the regional features of the main field, and their changes produce the secular magnetic variation. According to this theory, the geomagnetic field will remain of mainly dipole character nearly down to the surface of the core, with the lines of magnetic force lying nearly in planes through the geomagnetic axis. The magnetic intensity will increase inversely as the cube of the distance from the centre. There is a reaction between the magnetic field and the electric currents in the core, that tends to produce a westward drift of the core and hence of the secular magnetic variations relative to the outer solid part of the earth. This is reflected in a slow progressive, temporal change in all the geomagnetic elements (David, 1981).

Diurnal variations are small but more rapid oscillations in the earth's field with a periodicity of about a day and amplitude averaging 25 nT (Dobrin, 1988). The fast variations of magnetic field that takes place within the course of the day are connected with phenomena occurring on the sun. These variations are influenced by conditions in the atmosphere. The highly ionized layer of upper atmosphere above 80 km altitude which in turn is affected by the solar emissions. Normally, steady ring currents are present in the ionosphere. In addition the outer layers of the sun 'corona' erupt occasionally emitting corpuscular rays consisting of protons and electrons. When the corpuscles impinge upon the ionosphere, the ring currents are greatly disturbed and this affects the magnetic field of the earth (Fukushima and Kaminde, 1973).

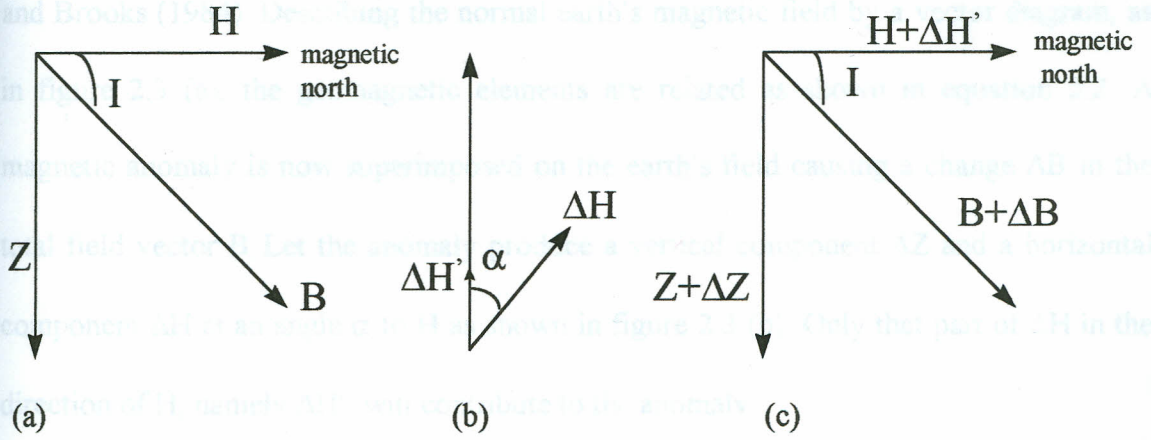

Figure 2.3 a, b and c Vector diagram representing the Earth's magnetic field (Kearey and Brooks, 1984).

The magnetic anomaly consists of that part of the magnetic field which is caused by irregularities in the distribution of magnetized material in the outer-crust of the earth. The magnetized rock produces a magnetic field around itself. If the rock is close enough to the earth's surface, its magnetic field will combine with the earth's field. The field from the rock constitutes the anomalous field and because fields are vectors, the combined field may be greater or smaller than the geomagnetic field acting alone. If the field from the magnetized body lies more or less in the same direction as the earth's magnetic field at the site, the two fields will reinforce each other, and the total field will be greater than the earth's field alone and the resulting anomaly is a positive anomaly. If the two fields are opposite in direction, they will cancel each other and the total field will be smaller than the earth's field alone the resulting anomaly being negative. A magnetic anomaly is detected when the measured magnetic field at the earth's surface differs from the undisturbed geomagnetic field. This implies presence of a magnetized material below the subsurface. All magnetic anomalies caused by rocks are superimposed in the main field of the earth. The description of the magnetic anomaly below was extracted from Kearey

and Brooks (1984). Describing the normal earth's magnetic field by a vector diagram, as in figure 2.3 (a), the geomagnetic elements are related as shown in equation 2.2. A magnetic anomaly is now superimposed on the earth's field causing a change ΔB in the total field vector B. Let the anomaly produce a vertical component ΔZ and a horizontal component ΔH at an angle α to H as shown in figure 2.3 (b). Only that part of ΔH in the direction of H, namely $\Delta H'$, will contribute to the anomaly.

$$\Delta H' = \Delta H \cos \alpha \tag{2.4}$$

Also,

$$(B + \Delta B)^2 = (H + \Delta H')^2 + (Z + \Delta Z)^2 \tag{2.5}$$

Expansion of the above equation ignoring the negligible terms in Δ^2 yields,

$$\Delta B = \Delta Z \, (Z/B) + \Delta H'(H/B) \tag{2.6}$$

Substituting the above equation with angular descriptions of geomagnetic element ratios yields,

$$\Delta B = \Delta Z \sin I + \Delta H \cos I \cos \alpha \tag{2.7}$$

The above approach can be used in calculating the magnetic anomaly caused by a small magnetic pole of strength m, defined as the effect of this pole on a unit positive pole at the observation point. The pole is situated at depth z, a horizontal distance x and radial distance r from the observation point and θ is the angle between a line joining the pole to the observation point to the horizontal as illustrated in figure 2.4.

The force of repulsion ΔBr on the unit positive pole in the direction r is given by,

$$F = \mu_o \, m_1 \, m_2 / 4\pi\mu_R r^2 \tag{2.8}$$

where m_1 and m_2 are magnetic poles of strengths m_1 and m_2 separated by a distance r and

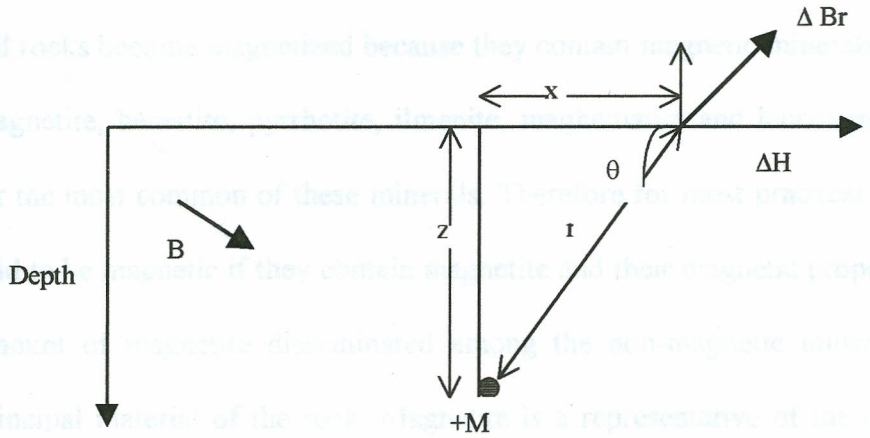

Fig.2.4 Magnetic pole of strength +M at distance r from observation point (Kearey and Brooks, 1984).

μ_o and μ_R are constants corresponding to the magnetic permeability of vacuum and relative magnetic permeability of medium separating the poles. The S.I unit for μ_o is Hm^{-1} and μ_R is dimensionless. Substituting $\mu_R = 1$ since relative permeability for air is close to unity then,

$$\Delta Br = Cm/r^2 \qquad (2.9)$$

where $C = \mu_0/4\pi$. Assuming the profile lies in the direction of magnetic north so that the horizontal component of the anomaly lies in this direction, then ΔB and ΔZ resolved in their relevant directions are given by,

$$\Delta H = Cm \cos\theta /r^2 = Cmx/ r^3 \qquad (2.10)$$

$$\Delta Z = - Cm \sin\theta/r^2 = -Cmz/r^3 \qquad (2.11)$$

$$\Delta B = -Cmz \sin I/r^3 + Cmx \cos I \cos\alpha/r^3 \qquad (2.12)$$

where α is zero if profile is in the direction of the magnetic north. If the converse is the case, α would represent the angle between the magnetic north and the profile direction.

2.3.3 Rock magnetism

All rocks become magnetized because they contain magnetic minerals. Such minerals are magnetite, hematite, pyrrhotite, ilmenite, maghematite and leucoxenes but magnetite is far the most common of these minerals. Therefore for most practical purposes, rocks are said to be magnetic if they contain magnetite and their magnetic properties depend on the amount of magnetite disseminated among the non-magnetic minerals making up the principal material of the rock. Magnetite is a representative of the cubic minerals with spontaneous magnetizations comparable to the familiar ferromagnetic metals (Fe, Co, Ni). Hematite is representative of the more weakly magnetic, uniaxial minerals, in which the oppositely magnetised sub-lattices of interacting Fe^{3+} ions are equally balanced that is anti-ferromagnetic but centered at a small angle to give slight spontaneous magnetization perpendicular to the ion moments. The magnetism of a rock may either be induced by the earth's field or remanent which may have occurred during cooling or deposition in the rock's history. The ionic moments of the magnetic domains in different type of materials determine their net spontaneous magnetization (Stacey, 1977). This is displayed in table 2.1

TYPE	EXAMPLE	IONIC MOMENTS	NET SPONTANEOUS MAGNETIZATION
Ferromagnetic	Fe,Co,Ni	↑ ↑ ↑ ↑	↑
Antiferromagnetic	NiO,MnO	↑ ↓ ↑ ↓	zero
Ferrimagnetic	Magnetite	↑ ↓ ↑ ↓	↑
Canted antiferromagnetic	Hematite	↗ ↖ ↗ ↖	→

Table 2.1 Basic patterns of alignment of atomic magnetic moments by mutual interaction (source: Stacey, 1977)

Induced magnetization refers to the action of the field on the material where the ambient field of the earth is enhanced and the material itself acts as a magnet. This magnetization is directly proportional to the intensity of the ambient field.

$$I_i = kF \tag{2.13}$$

where k is the volume magnetic susceptibility, F the ambient field intensity and I_i is the induced magnetization per unit volume. The magnetic susceptibility of a rock containing magnetite is simply related to the amount of magnetite it contains. The remanent magnetization I_r is a permanent magnetization often predominant in many igneous rocks. This magnetization depends upon thermal, mechanical and magnetic history of the material and is independent of the field in which it is measured. Before such heating, the domains within each magnetite crystal are randomly oriented. During heating at high temperature, the domains reorient themselves, which upon cooling tend to align themselves in the direction of the earth's field present at that time. The remanent magnetization of a rock may not be in the same direction as the present earth's field for the field is known to have changed its orientation in geologic time. Sediments that are accumulations of debris from weathering of igneous rocks frequently contain grains of magnetite whose magnetic moments are partially aligned by the earth's field during or immediately after deposition and thus impart a detrital remanent magnetization (DRM) to the deposit. However the process of compaction and solidification of sediments are frequently accompanied by chemical changes in which at least some magnetite is oxidized to hematite. The hematite is formed chemically at low temperature in the earth's field and if the grain size becomes large enough it may acquire chemical remanent magnetization (CRM) in the process. The intensities of natural remanent magnetization

(NRM) for most rocks that are of thermal or chemical origin cover a wide range but most are between 10 and 10^{-4} AM^{-1}. However, rocks normally acquire secondary magnetizations superimposed on the original or primary magnetization. Secondary magnetizations have a number of causes e.g. effects of currents due to lightning. Mild re-heating may introduce a low temperature TRM, or isothermal exposure to a field over geological time may cause viscous magnetization of less stable magnetic constituents (Stacey, 1977).

CHAPTER 3

3 FIELD STUDIES

3.1 GROUND MAGNETIC SURVEY

3.1.1 Introduction

The fieldwork was carried out in Magadi Division of Kajiado District which is in the southern part of the Kenya Rift system. The study area covers 351 sq kms located between latitudes 1°48′S to 2°2′S and longitudes 36°14′E to 36°23′E. A ground magnetic survey was carried out as from January to March 1998. A total of 53 Magnetic stations where established in the area of study with a spacing of about 1 Km apart. In each particular day repeated measurements were made in a base station. Some of the pre-existing KRISP 94 gravity stations were also used as magnetic stations for the survey. A few stations where established along the cause way and none in the lake. The soda in the lake had dissolved due to the El-Nino rains making the lower part of the lake inaccessible. The network of stations established are displayed in figure 3.1. Altitude measurements were unnecessary for their effect on the vertical magnetic field was assumed negligible since the terrain in study area was relatively flat. Temperature measurement was not necessary since the flux-gate magnetometer used does not drift and hence the magnetic reading made was not a function of temperature. With exception of the Eastern part of lake Magadi on the plain extending to Karamai, shown in figure 1.1 the selection of sites for magnetic stations was mainly confined near motorable roads. This was done to allow easy and fast return to the base station for diurnal variation measurements also making wide coverage of stations possible within a day.

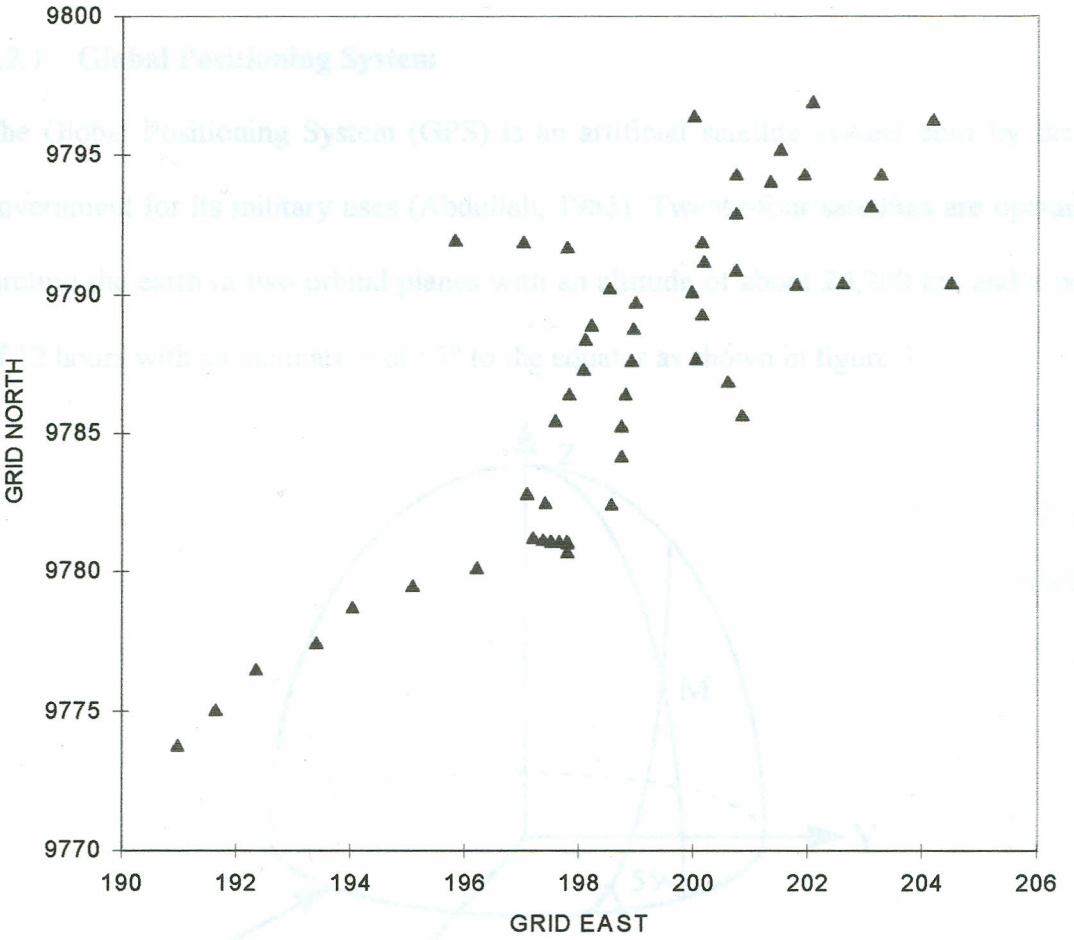

Figure 3.1 Distribution of magnetic stations in the study area

The stations were positioned at a safe distance of at least 50 metres from magnetic objects such as bridges, tarmac roads and railway lines. Magnetometers may fail to give consistent readings near high voltage power lines due to the production of high noise level. The same safe distance of at least 50 metres was maintained from such lines to the magnetic stations. Establishment of stations on outcropping volcanic lava was avoided due to their high percentage of ferromagnetic minerals.

3.2 FIELD INSTRUMENTS

3.2.1 Global Positioning System

The Global Positioning System (GPS) is an artificial satellite system built by the U.S government for its military uses (Abdullah, 1985). Twenty-four satellites are operational circling the earth in two orbital planes with an altitude of about 20,200 km and a period of 12 hours with an inclination of 55° to the equator as shown in figure 3.2.

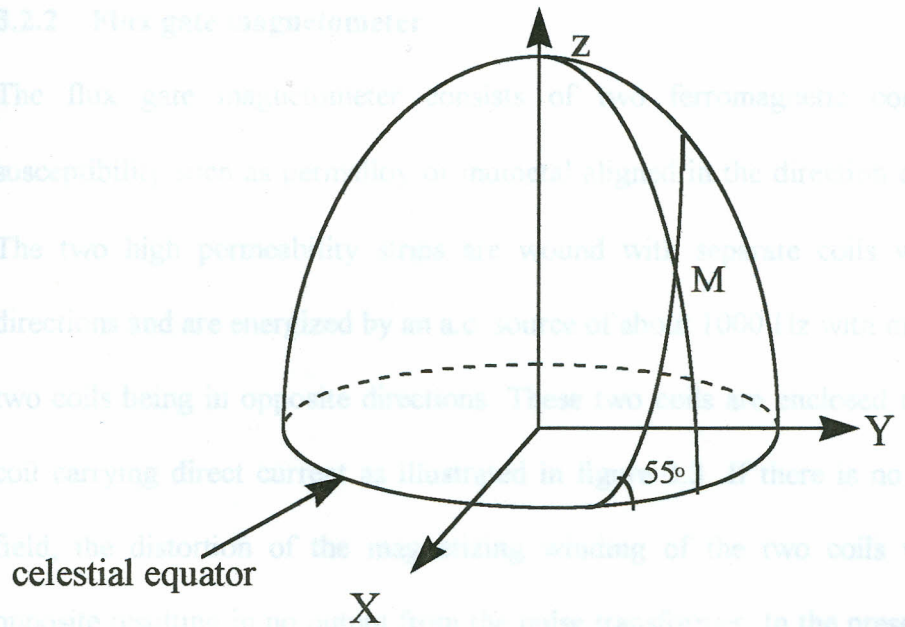

Figure 3.2 An artificial satellite M circling the earth.

The artificial satellites transmit signals of high frequencies giving the position of the satellite in space. The high frequency signals minimize the effects of ionospheric refraction making positioning more precise. This information is received by a receiver placed at the point whose position is to be determined. The satellite receiver tracks and records every available pass at a given location. This data are fed to a computer program

which combines all the raw data to obtain the single best position fix result in 3-D that is latitude, longitude and altitude.

The GPS is essential for positioning in resource exploration. It has been proved to be a quick, reliable and cheaper tool compared to the former surveying positioning techniques. It is also not affected by physical limitations such as visibility, weather or time of the day.

3.2.2 Flux gate magnetometer

The flux gate magnetometer consists of two ferromagnetic cores of very high susceptibility such as permalloy or mumetal aligned in the direction of the earth's field. The two high permeability strips are wound with separate coils wound in opposite directions and are energized by an a.c. source of about 1000 Hz with magnetization of the two coils being in opposite directions. These two coils are enclosed together in another coil carrying direct current as illustrated in figure 3.3. If there is no external magnetic field, the distortion of the magnetizing winding of the two coils will be equal and opposite resulting in no output from the pulse transformer. In the presence of an ambient magnetic field, the hysteresis curves for the two strips are displaced in opposite directions. The pulses from the two windings no longer balance each other and there is a net output pulse to the amplifier. This output is directional and changes sign when the ambient field changes sign. The net output pulse is proportional to the ambient field intensity at the magnetometer element. This net output activates a balancing circuit, which changes the current in the d.c coil bring the net field to zero. The change in the d.c balancing current is recorded digitally (Nettleton, 1976).

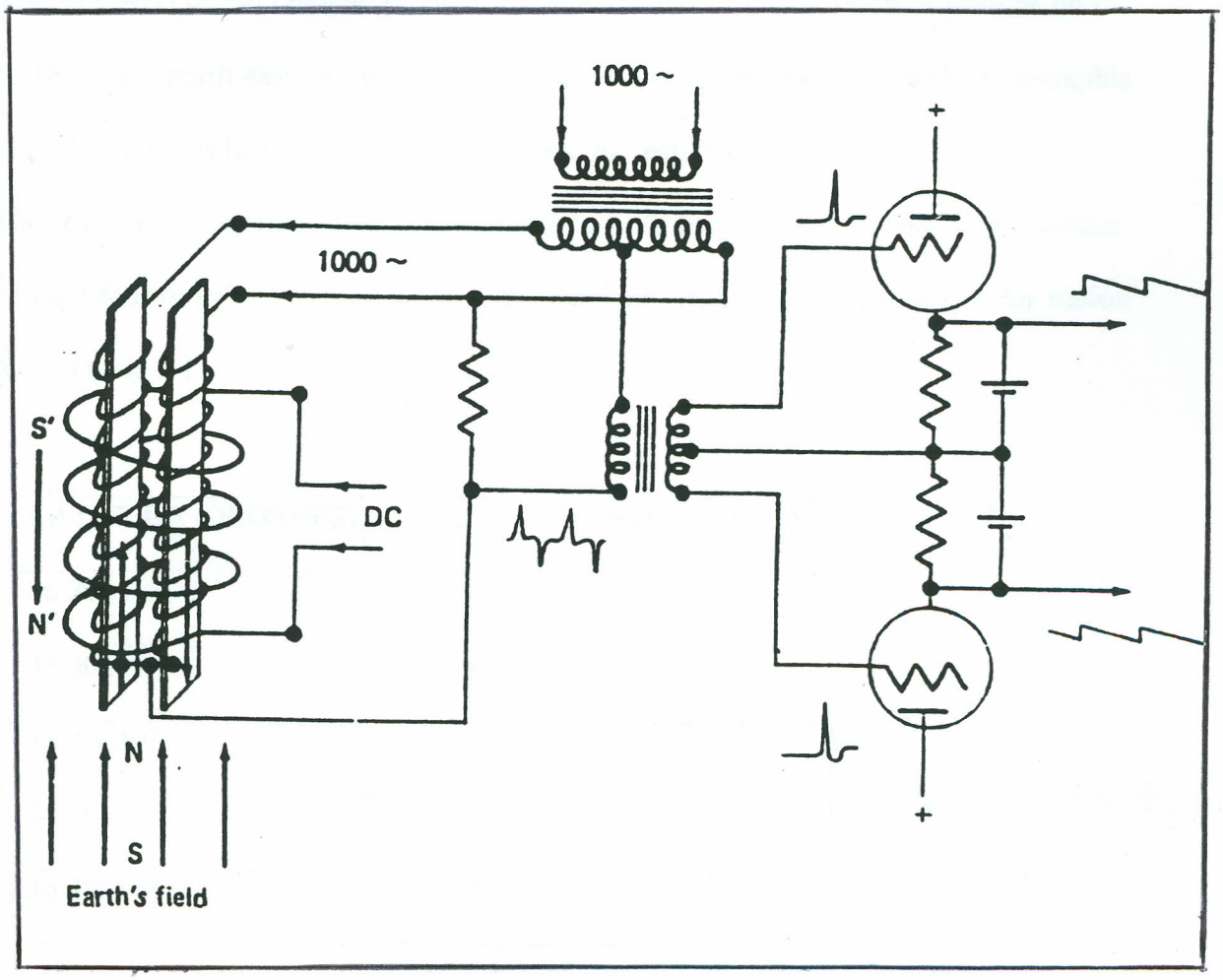

Fig. 3.3 Schematic diagram of the flux-gate Magnetometer (after Nettleton, 1976)

3.3 Field measurements

The positioning of most established stations was measured using a Global Positioning System (GPS) model Garmin 45 described in section 3.2. The position of stations on the northern and north-eastern part of the study area were interpolated from the topographic map. The stations had been established at existing features visible on the map.

The reading of the position was made after the GPS had received at least five satellites. At least four repeated readings were made and their mean computed as shown for station A10 in table 3.1

LATITUDE (DEGREES)	LONGITUDE (DEGREES)
36.306533	1.883366
36.306516	1.883300
36.306300	1.883200
36.306333	1.883116
36.306333	1.883466

Table 3.1 Repeated GPS readings at station A10

The GPS readings made in a particular station oscillated around the mean point of co-ordinates (36.306403, 1.883289) as an ellipse. The standard deviation of the latitude and longitude were 1.119×10^{-4} and 1.371×10^{-4}. This is illustrated in figure 3.4 using the repeated GPS readings taken at station A10.

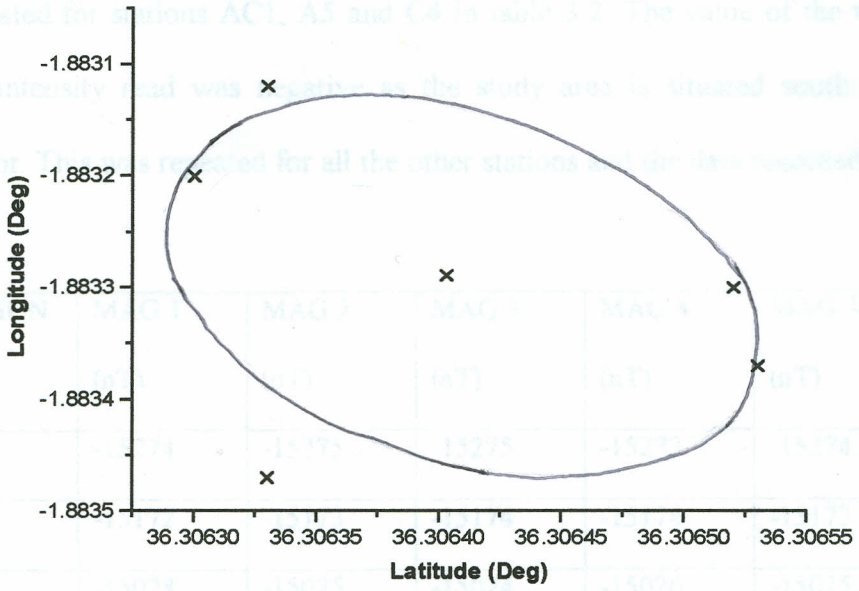

Figure 3.3 A plot of repeated GPS readings at station A10

The position co-ordinates for the stations obtained as latitude and longitudes were later converted to traverse Mercator grid co-ordinates using a computer program DEGREC (Stangl, personal communication) derived from equations in Appendix 1. The values of false easting, false northing, central meridian and scale factor used in the program for the study area were extracted from the topographical map of Magadi sheet 160/4.

The vertical magnetic field component was measured at each station with a digital flux gate magnetometer model MFD-2 Scintrex whose operation is briefly described in section 3.2. In each day the measurements along a particular profile were repeated at the base station after at most two hours interval which was necessary for carrying out corrections of the diurnal variations. Four readings of the vertical magnetic field intensity

were measured at each established station and the mean, and standard error determined as illustrated for stations AC1, A5 and C4 in table 3.2. The value of the vertical magnetic field intensity read was negative as the study area is situated south of the magnetic equator. This was repeated for all the other stations and the data recorded in Appendix 2.

STATION	MAG 1 (nT)	MAG 2 (nT)	MAG 3 (nT)	MAG 4 (nT)	MAG AVE (nT)	±
AC1	-15274	-15275	-15275	-15273	-15274.3	0.4787
A5	-15172	-15173	-15174	-15174	-15173	0.4083
C4	-15028	-15025	-15024	-15026	-15025.8	0.8539

Table 3.2 Magnetic intensity measured at stations AC1, A5 and C4

CHAPTER 4

4 DATA PROCESSING

4.1 INTRODUCTION

Prior to mapping, the raw observed magnetic data must be corrected to eliminate the effects of the earth's main field and the diurnal variations. The International Geomagnetic Reference Field (I.G.R.F) is a mathematical model of the earth's main field with its temporal variations and consists of a series of spherical harmonics based on world wide magnetic observatory data. In practice, for magnetic surveys the I.G.R.F updated to the time of survey is subtracted from the observed magnetic field data to remove the non-crustal effects from the data. The diurnal variations cannot easily be approximated by a mathematical model (Dobrin, 1988). Diurnal variations are subject to amplitude and phase changes depending on the geographical location of the observer and can be influenced by geological conditions such as rock susceptibility at the place of observation. After removal of the I.G.R.F and diurnal variations from the measured magnetic field data only the effect of the residual magnetic anomalies solely due to geology remain.

4.2 GROUND MAGNETIC DATA REDUCTION

The magnetic field readings are affected by the sum of all contributions to the magnetic field at the time and place of observation. The main aim of the survey is to map the anomaly part of the vertical magnetic field. Thus, it is necessary to remove the extra effects to attain a true image of the local magnetic anomalies. The raw observed data set presented in Appendix 2 were reduced by the following procedure:

All the four field measurements of magnetic field observed in any particular station were averaged and the mean value recorded. Station B1 was taken as the base station on all the days except on 21/1/98 and 1/2/98. Readings of the vertical magnetic intensity were measured at B1 after every 2-3 hours. Before going back to the base stations, repeated readings were also taken in some of the occupied magnetic stations, whose diurnal curve was drawn and shifted to merge with diurnal curve due to station B1. On 21/1/98, station A2 was used as the base station and by repeating readings in A3, a diurnal curve was made using A2 as the base station and the curve due to A3 shifted to fit diurnal variation curve due to A2. On 1/2/98, station B5 was used as the base station and its diurnal curve plotted.

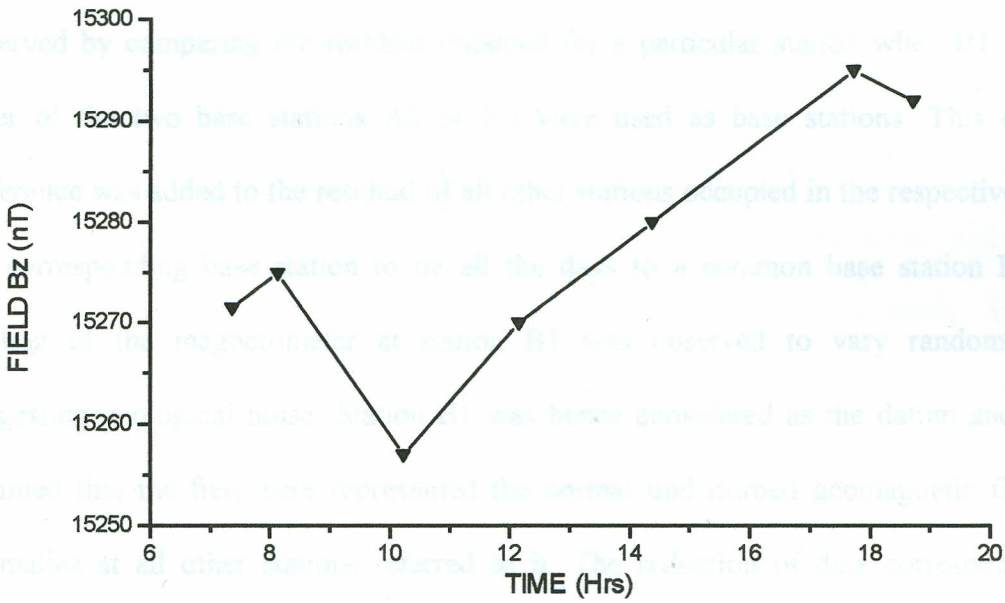

Figure 4.1 Diurnal variation curve for 28/3/98 at base station B1

The repeated base station magnetic readings were plotted against their time of observation with the assumption of a linear variation in between stations. These diurnal variation curves corresponding to the respective days of the survey were plotted in Fig.4.1 as monitored on 28/3/98. Base station readings corresponding in time to the observed field readings were interpolated from the diurnal variation curves and recorded as displayed in Appendix 2. The interpolated base station readings were subtracted from the observed field data resulting in a residual field with dc components of the main field removed (Dobrin, 1988).

The difference in the residual anomaly of a repeated station when base station B1 and the base stations A2 and B5 used in the two days was determined. A constant difference was observed by comparing the residual obtained for a particular station when B1 and any other of the two base stations A2 or B5 were used as base stations. This constant difference was added to the residual of all other stations occupied in the respective day of the corresponding base station to tie all the days to a common base station B1. The reading of the magnetometer at station B1 was observed to vary randomly only suggesting geological noise. Station B1 was hence considered as the datum and it was assumed that the field here represented the normal undisturbed geomagnetic field and anomalies at all other stations referred to it. The reduction of data corresponding to stations B5, B9 and A18 is illustrated in table 4.1. Thus both the diurnal and geomagnetic corrections were made and only the regional trend remained.

STATION	B5	B9	A18
TIME	12.45	16.49	12.43
MEANMAGNETIC FIELD (nT)	-15169.50	-15341.75	-15107.00
BASE MAGNETIC FIELD (nT)	-15370.00	-15360.00	-15300.00
RESIDUAL FIELD (nT)	+200.50	+18.25	+193

Table 4.1 Data reduction at stations B5, B9 and A18

The reduced vertical magnetic intensity data was regularized in a rectangular grid and contoured by use of Surfer software as displayed in figure 4.2 where the solid and hachured contours represents positive and negative anomalies respectively. Figure 4.2 is the reduced vertical magnetic intensity contour map which displays the magnetic anomalies in the study area. The anomalies have a N-W, S-E trend which is very likely influenced by the station distribution. The 3-D surface plot of the residual magnetic intensity in the study area is illustrated in figure 4.3 where the crests and troughs represents areas of positive and negative magnetic anomalies respectively. The final reduced magnetic data set is presented in Appendix 2. Stations judged to have bad data values (based on surrounding data) marked with asterix were not used in contouring.

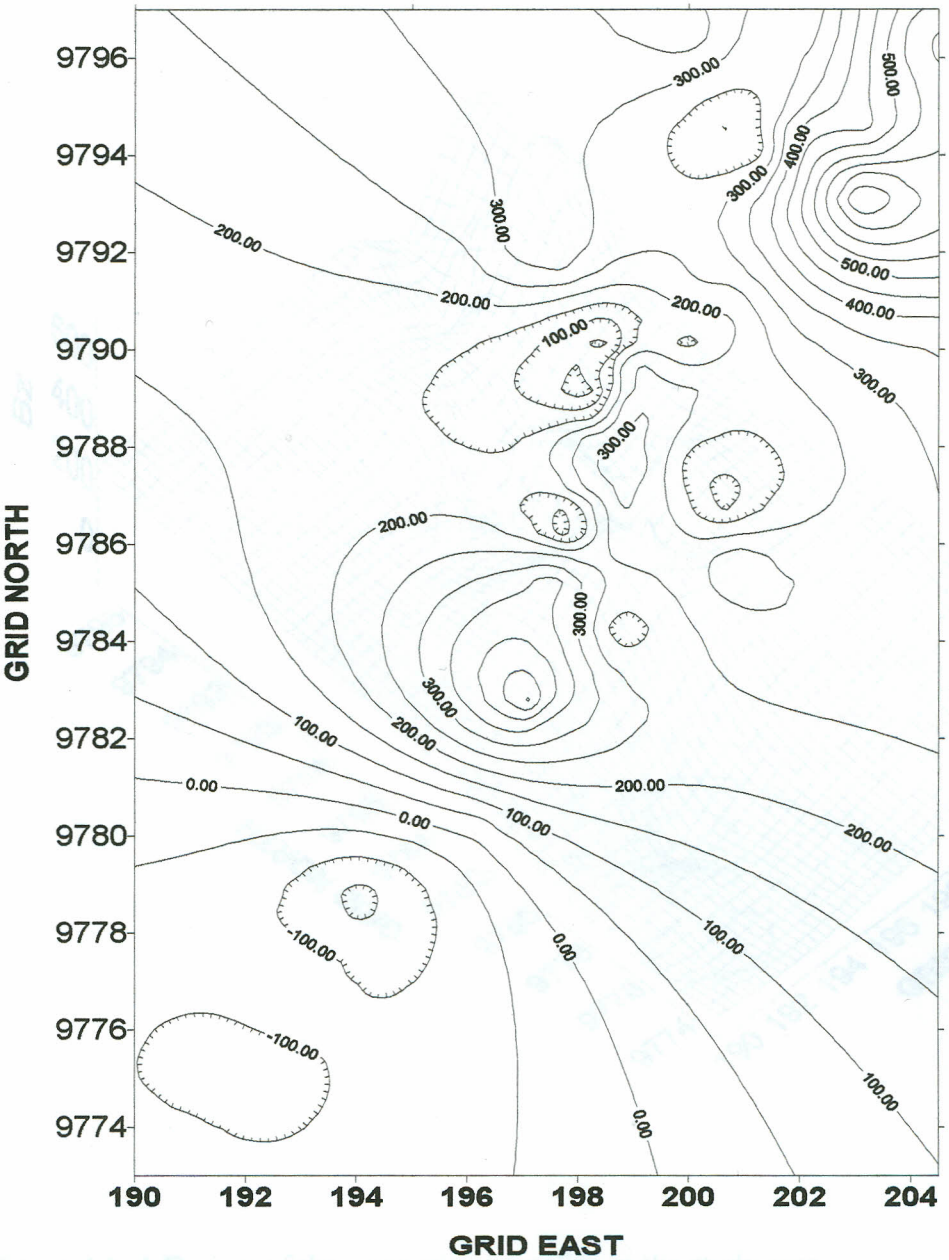

Figure 4.2. Reduced vertical magnetic intensity contour map

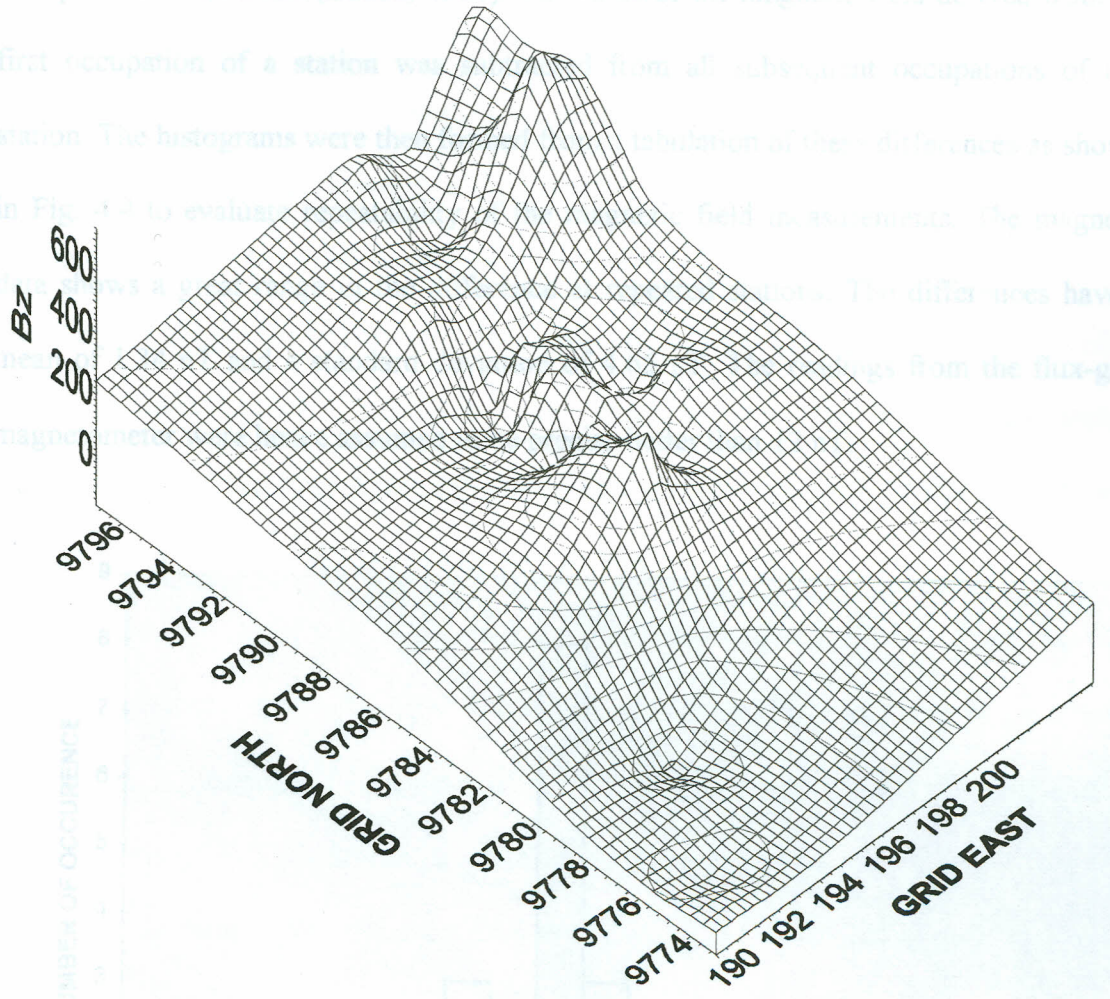

Figure 4.3. 3-D view of the magnetic anomalies in the study area

4.2.1 Accuracy criteria of final data

The accuracy criterion used here is the differences in the data acquired by repeated occupations of a station (Edcon, 1986). The value of the magnetic field derived from the first occupation of a station was subtracted from all subsequent occupations of that station. The histograms were then formed from a tabulation of these differences as shown in Fig. 4.4 to evaluate repeatability of the magnetic field measurements. The magnetic data shows a great range in the difference at repeated stations. The differences have a mean of 1.34 nT and a standard deviation of 4.65 nT. The readings from the flux-gate magnetometer were hence assumed to be precise better than ±2 nT.

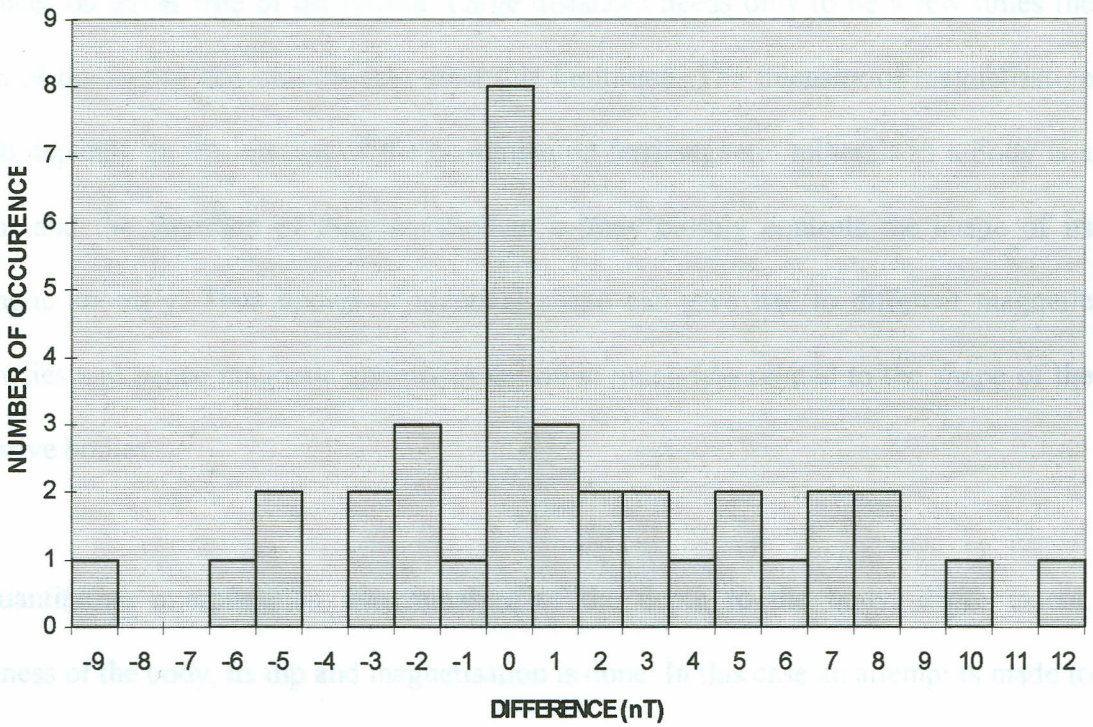

Fig.4.4 A Histogam illustrating accuracy of final data

CHAPTER 5

5 INTERPRETATION OF GROUND MAGNETIC DATA

5.1 INTRODUCTION

Potential field data can be interpreted either in map form as in Fig. 4.1 or from selected profiles as in the Fig. 5.1. The map represents the total picture and no assumptions regarding strike and lateral extent of the causative source need to be made. From the map, anomalous regions can be detected and the subsurface structure known from the anomaly pattern. Quantitative interpretation which involves analysis of magnetic anomaly profiles allows the interpretation of data as recorded. Direct interpretation methods must assume that the profiles are normal to the strike direction and that the bodies extend large distances on either side of the profile. Large distances needs only to be a few times the depth of the source and most bodies meet this limitation. The intensity of magnetisation which depends on the amount of the disseminated ferrimagnetic minerals in a body is a vector and the direction of magnetisation in a body closely controls the shape of its magnetic anomaly. Thus bodies of identical shape can give rise to different magnetic anomalies and hence magnetic anomalies are often much less related to the shape of the causative bodies.

In quantitative interpretation determination of the depth to the body, depth extent, thickness of the body, its dip and magnetisation is done. In this case an attempt is made to match the observed anomaly with that calculated for a model by iterative adjustments to the model. The problem of ambiguity in magnetic interpretation is common and hence controls on the nature and form of the causative body must be employed to reduce it.

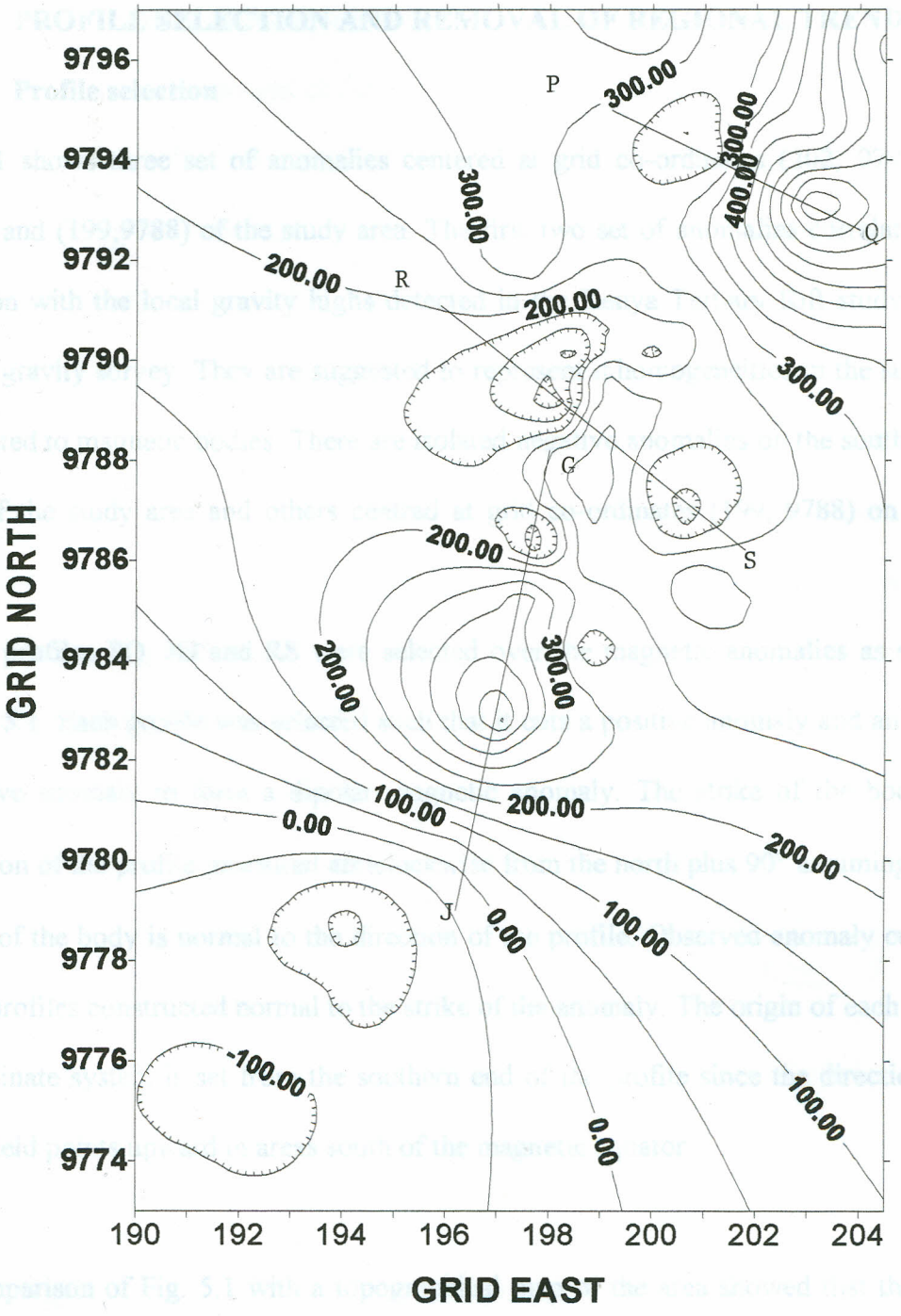

Figure 5.1. Vertical intensity map with the selected profiles

5.2 PROFILE SELECTION AND REMOVAL OF REGIONAL TREND

5.2.1 Profile selection

Fig.5.1 shows three set of anomalies centered at grid co-ordinates (202, 9794), (197, 9784) and (199,9788) of the study area. The first two set of anomalies correlate well in position with the local gravity highs detected in the Kenya Tertiary Rift study (Beicip, 1987) gravity survey. They are suggested to represent inhomogeneities in the subsurface attributed to magnetic bodies. There are isolated negative anomalies on the south-western part of the study area and others centred at grid co-ordinates (199, 9788) on the lake floor.

Three profiles PQ, JG and RS were selected over the magnetic anomalies as shown in figure 5.1. Each profile was selected such that it cuts a positive anomaly and an adjacent negative anomaly to form a dipolar magnetic anomaly. The strike of the body is the direction of the profile measured anticlockwise from the north plus 90° assuming that the strike of the body is normal to the direction of the profile. Observed anomaly curves are from profiles constructed normal to the strike of the anomaly. The origin of each profile's co-ordinate system is set from the southern end of the profile since the direction of the total field points upward in areas south of the magnetic equator.

A comparison of Fig. 5.1 with a topographical map of the area showed that there is no marked correlation of the terrain with the magnetic anomalies. This suggests that the sources of the magnetic anomalies may not be a factor of terrain.

5.2.2 Calculation of residual anomalies

The regional is the component of the magnetic anomaly having long wavelength and low spatial frequency. The anomaly with short wavelength and high spatial frequency superimposed on it is the residual anomaly. This occurs when the lateral extent of one anomaly is greater than the other. The sources of the regional trends are large geological structures or intra-basement lithologic changes. The residuals have to be isolated from the regional by high pass spatial frequency filtering. Considering the survey area to be small, trend analysis was used to remove the regional field. In this case the regional field is approximated by a linear trend. A trend line for profile data is fitted to the observations and subsequently subtracted from the observed reduced magnetic anomaly data. This is illustrated by figures 5.2 a-c which represents isolation of the residual field from profiles P-Q, J-G and R-S.

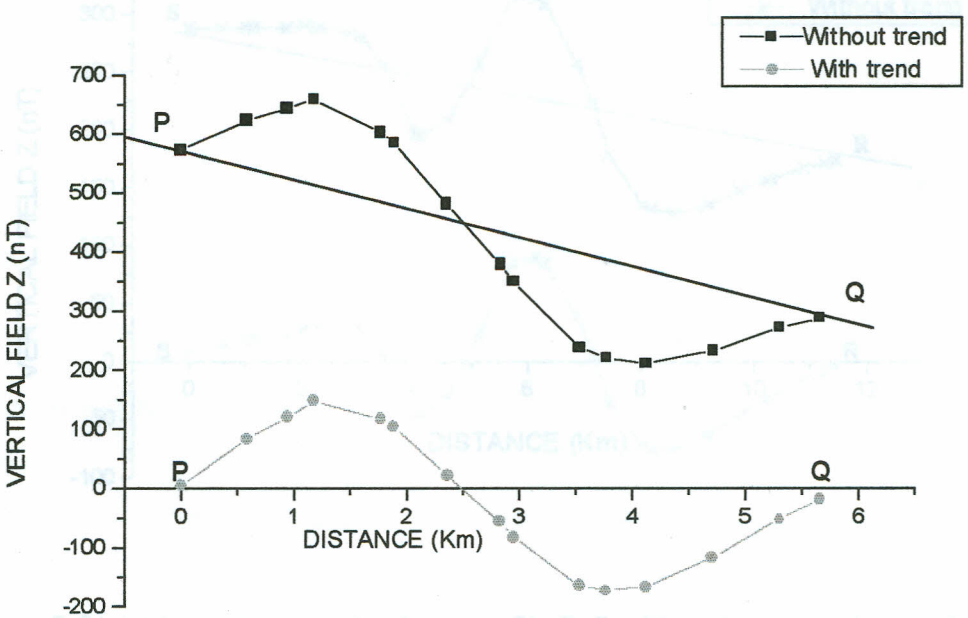

Figure 5.2(a) Magnetic anomaly along profile P-Q with and without the trend.

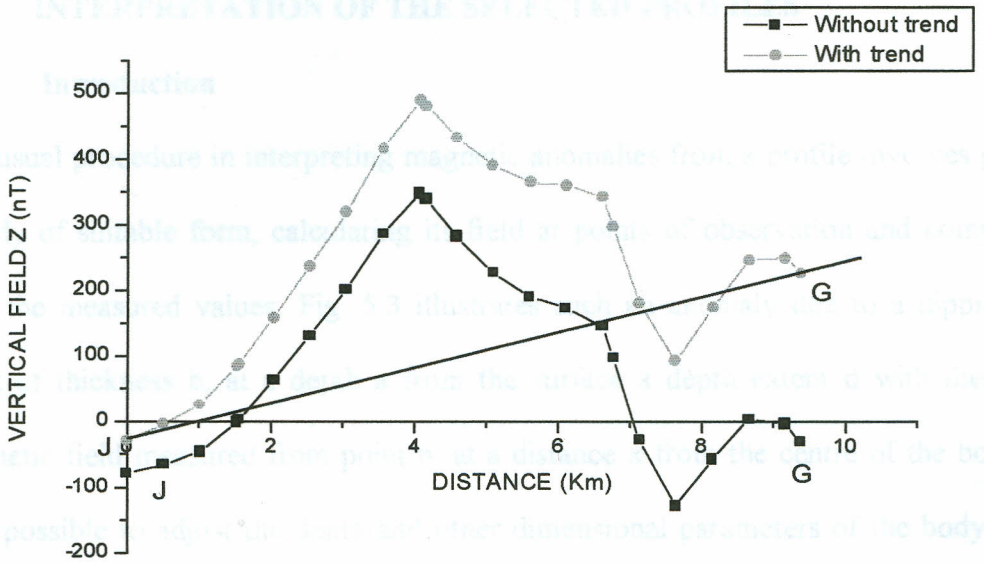

Figure 5.2(b) Magnetic anomaly along profile J-G with and without the trend.

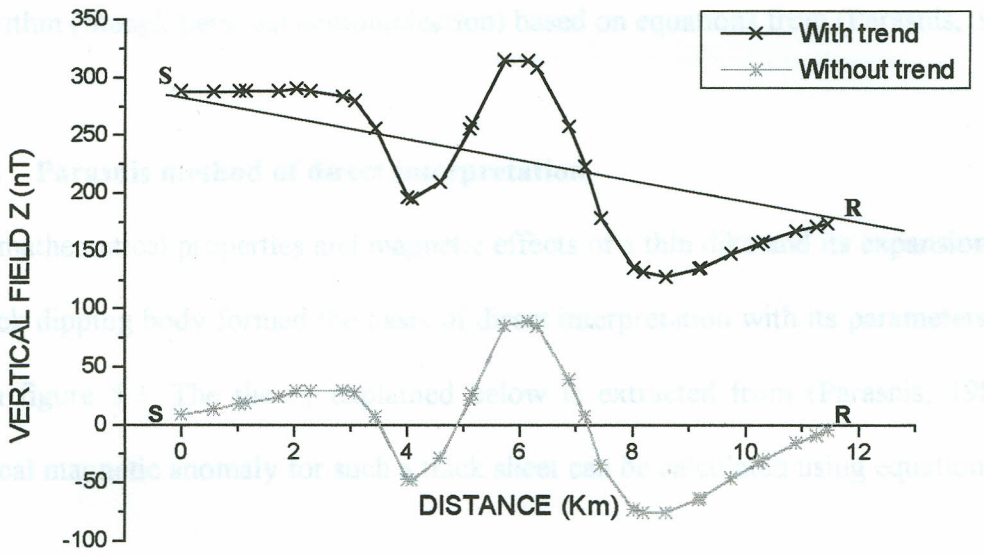

Figure 5.2(c) Magnetic anomaly along profile R-S with and without the trend.

5.3 INTERPRETATION OF THE SELECTED PROFILES

5.3.1 Introduction

The usual procedure in interpreting magnetic anomalies from a profile involves guessing a body of suitable form, calculating its field at points of observation and comparing it with the measured values. Fig. 5.3 illustrates such an anomaly due to a dipping thick sheet of thickness b, at a depth a from the surface a depth extent d with the vertical magnetic field measured from point p. at a distance x from the centre of the body. It is then possible to adjust the depth and other dimensional parameters of the body by trial and error or by automatic optimizing methods until a satisfactory agreement is achieved between the calculated and the observed values. This agreement in practice should be along one or more selected profiles and not over the entire area (Parasnis, 1986). Both direct interpretation and forward modelling have been carried out using MAGCALC algorithm (Stangl, personal communication) based on equations from (Parasnis,1986)

5.3.2 Parasnis method of direct interpretation

The mathematical properties and magnetic effects of a thin dike and its expansion to form a thick dipping body formed the basis of direct interpretation with its parameters defined as in figure 5.3. The theory explained below is extracted from (Parasnis, 1986). The vertical magnetic anomaly for such a thick sheet can be calculated using equation 5.1.

$$\Delta B_Z = (\mu_0/2\pi)\, M_r'\, C \sin\theta \,(\cos^{-1}((r_1^2+r_2^2-b^2)/2r_1r_2) - K \ln(r_1/r_2)) \qquad (5.1)$$

where a is depth of the body from the surface, b is its thickness, d is its depth extent, μ_o is permeability in vacuum and M_r' is the projection of magnetization in the direction of the strike. Distances r_1 and r_2 in Fig.5.4. can be calculated from equations 5.1 and 5.2.

$$r_1 = ((x+ b/2)^2 + a^2)^{1/2} \quad (5.2)$$

$$r_2 = ((x- b/2)^2 + a^2)^{1/2} \quad (5.3)$$

and constants C and K are given by:

$$C = \cos (\theta - i') \quad (5.4)$$

$$K = \tan (\theta - i') \quad (5.5)$$

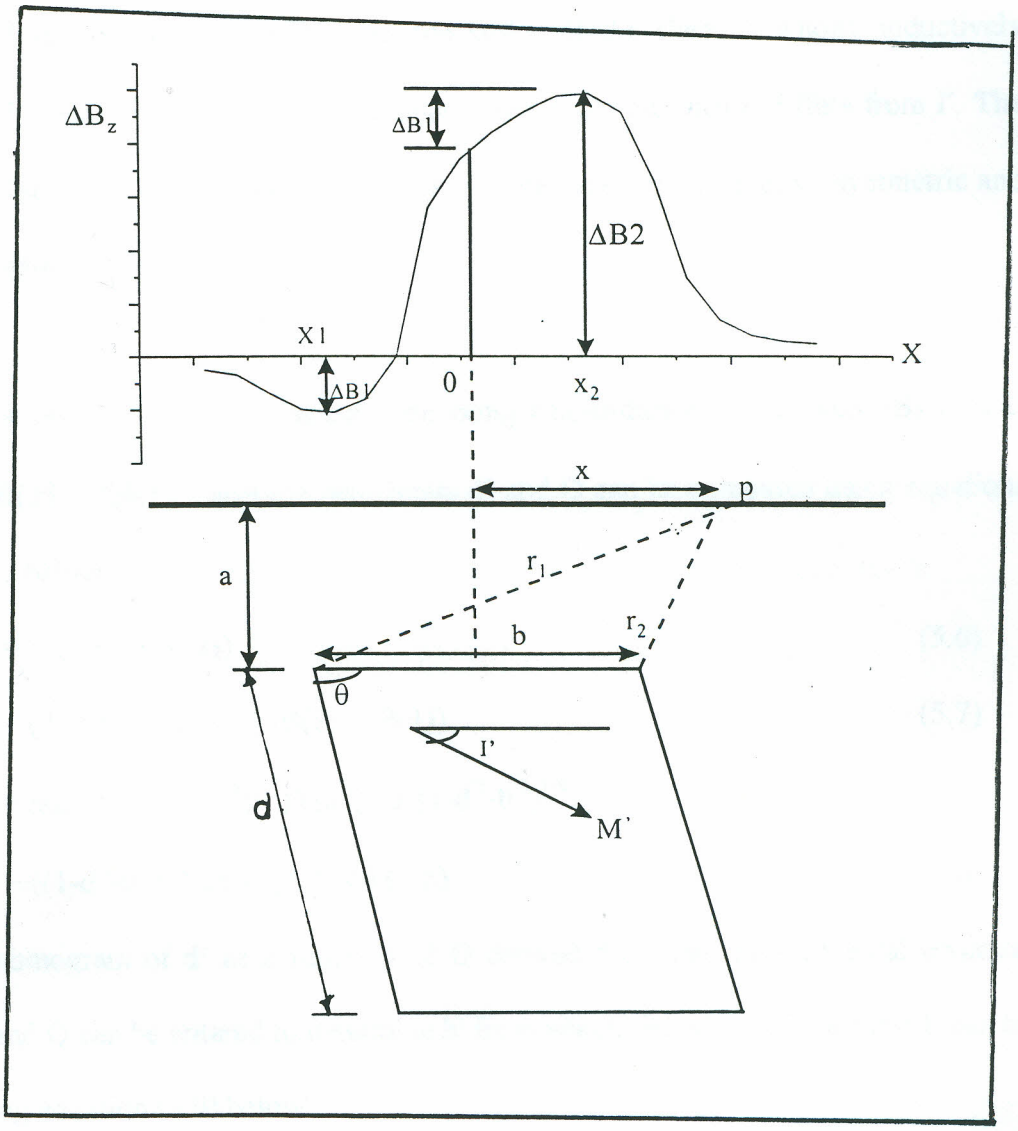

Figure 5.3 Features of magnetic profile across a thick sheet (Parasnis D.S., 1986)

From the magnetic anomaly curve figure 5.3, ΔB1 and ΔB2 denotes the extreme values of ΔB where ΔB2 is numerically the greater of the two, and the corresponding distances X_1 and X_2 measured from the origin 0 as shown in figure 5.4. X_1 should be the numerically greater value of the two.

It has been considered and i' is the inclination of vector M_r' and I'is the projection of the earth's inclination I in the direction of the strike. If the sheet is wholly inductively magnetized, then $i' = I'$ and if it has remanent magnetisation, then i' differs from I'. The three possible types of anomalies that can be obtained are non-symmetric, symmetric and anti-symmetric.

For a non-symmetric magnetic anomaly, denoting x co-ordinates of ΔB_1 and ΔB_2 with $x_1 > x_2$ if $|\Delta B(2)| > |\Delta B(1)|$, then the parameters d' and Q can be computed using equations 5.6 and 5.7 below.

$$d' = (x_1 + x_2)/(x_1 - x_2) \tag{5.6}$$

$$Q = (\Delta B(2) + \Delta B(1))/(\Delta B(2) - \Delta B(1)) \tag{5.7}$$

$$Q = \tan^{-1}(b'/(1-d'^2-b'^2)^{1/2})/\tan^{-1}(b'd'/(1-d'^2-b'^2)^{1/2}) + ((1-d'^2-b'^2)^{1/2}/2d')\log((1+b')/(1-b)) \tag{5.8}$$

Using a nomogram of d' as a function of Q derived from the transcendental equation (5.8), d' and Q can be entered to determine b' from which the width of the sheet b can be found using equation (5.9) below.

$$b' = b/|x_1 - x_2| \tag{5.9}$$

Knowing b, the depth to the causative body a can be calculated from the equation (5.10) below.

$$a = (-x_1 x_2 - b^2/4) \quad (5.10)$$

For a symmetric anomaly, $|x_{1/2}|$ and $|x_{1/4}|$ denoting absolute values of the co-ordinates of the points at which ΔB_Z falls to one half and one fourth of the central value are used to compute a parameter ε as in equation (5.11) which is important in the determination of depth of the body from the surface (a) as in equation (5.12).

$$\varepsilon = x_{1/4} / x_{1/2} \quad (5.11)$$

$$a = (\varepsilon^2 - 1)\, x_{1/2}/2 \quad (5.12)$$

For an anti-symmetric anomaly profile, $x_1 \approx - x_2$ and $\Delta B1 \approx -\Delta B2$. If the co-ordinate $x_{1/2}$ at a point on which the anomaly is one half of one of the two extreme values is interpolated then, the ratio η as in equation (5.13) is used to determine thickness b as shown in equation (5.14).

$$x_1 / x_{1/2} = \eta \quad (5.13)$$

$$b^2 = (1+\eta^2)(4\eta - 1 - \eta^2)\, x_{1/2}^2 \quad (5.14)$$

The corresponding depth to the causative body is obtained from equation (5.10) above and constant K is obtained from equation (5.15) below.

$$K = 2a/(x_1 + x_2) \quad (5.15)$$

and $(\theta - I')$ can be determined from equation (5) assuming $i' = I'$. If the value of θ lies outside the range $0 \leq \theta \geq 180^\circ$, a suitable multiple of 180° is added or subtracted to give the correct angle θ.

The magnetization intensity M_r' when the profile is not perfectly antisymmetric is determined from equation (5.16).

$$(\mu_0/2\pi)\, M_r' \, C\sin\theta = (\Delta B(1)+\Delta B(2))/2\tan^{-1}(b/2a) \qquad (5.16)$$

For a nearly anti-symmetric magnetic anomaly profile, C becomes zero and hence M_r' can be found from equation (5.17).

$$(\mu_0/2\pi)\, M_r' \, \sin\theta = -\Delta B(1)/\ln((2x_1+b)/(2x_1-b)) \qquad (5.17)$$

From the above equation (5.17), knowledge of the normal geomagnetic field B_0 is not necessary to obtain M_r' but if it is known, the effective susceptibility can be found from equation (5.18).

$$M_r' = kT_0' = k(B_0'/\mu_0) \qquad (5.18)$$

For direct interpretation, the MAGCALC program computes a new origin from which distances X_1 and X_2 are measured as shown in figure 5.3. The input data and information necessary for direct interpretation when using MAGCALC includes the type of symmetry of the anomaly, ΔB_Z values versus distance measured in field co-ordinates for a particular profile, component of the field measured, strike direction of the body, total field and inclination of the study area. The values of the total field and earth's inclination of the study area used in the program are 35000nT and as -25° respectively. In this interpretation, the depth extent of the body was assumed to be infinity. Depending on the symmetry of profile the program MAGCALC computes parameters such as depth to the body a, dip of the body θ, magnetisation M_r', offset distance X_0 and the effective susceptibility using equations 5.6-5.18. The direct interpretation results of the profile data sets J-G, P-Q and R-S are displayed in table (5.1)

PROFILE	a(km)	b (km)	Dip(deg)	M_r' (AM^{-1})	Strike (deg)	k
P-Q	1.15	1.1239	55.73°	1.22	150°	0.0706
J-G	1.09	2.5019	84.35°	1.26	83°	0.0455
R-S(body1)	0.49	0.2853	79.89°	0.34	144°	0.0180
R-S(body2)	0.44	1.4773	46.29°	0.43	144°	0.0225

Table 5.1 Direct interpretation from the selected profiles

5.3.3 Forward Modelling

The values of the various parameters obtained in direct interpretation give estimates and can be adjusted further to get a possible agreement between the measured and calculated anomalies along a profile (Parasnis, 1986). The main aim of forward modelling is to obtain the depth extent of the body and to improve the body parameters obtained in the start model. Forward modelling was done using the MAGCALC program with the magnetic anomaly model curve computed using equations 5.1-5.5. The initial start model used for each profile derived from the results of direct interpretation and also the distance of fit are the necessary input information for forward calculation. Modelling was done iteratively by modifying source body configuration and magnetic parameters after each computation until a 'best fit' is obtained between the observed and calculated data curves of each model profile. Other than modifying the parameters acquired in direct interpretation, the depth extent of the bodies was determined by forward calculation. The decision on how to adjust the model at each iteration in trial and error was subjective.

Profile P-Q

The magnetic anomaly profile P-Q is oriented in a NW-SE. The profile was used to model the magnetic anomaly approximately centred at grid co-ordinates (202,9793). It was noted that the maximum depth to the top of the body that gave the best fit for the computed and the observed anomalies along profile P-Q was 1km. The computed values for the model along this profile shows that the width of the magnetic body is 2.2 km wide extending to a depth of 1.99 km. Its magnetization M_r' and dip to the horizontal were interpreted as 1.55 AM^{-1} and 78° respectively. Figure 5.4(a) shows the fit between the observed and the computed magnetic anomaly curves along the profile P-Q together with the source body.

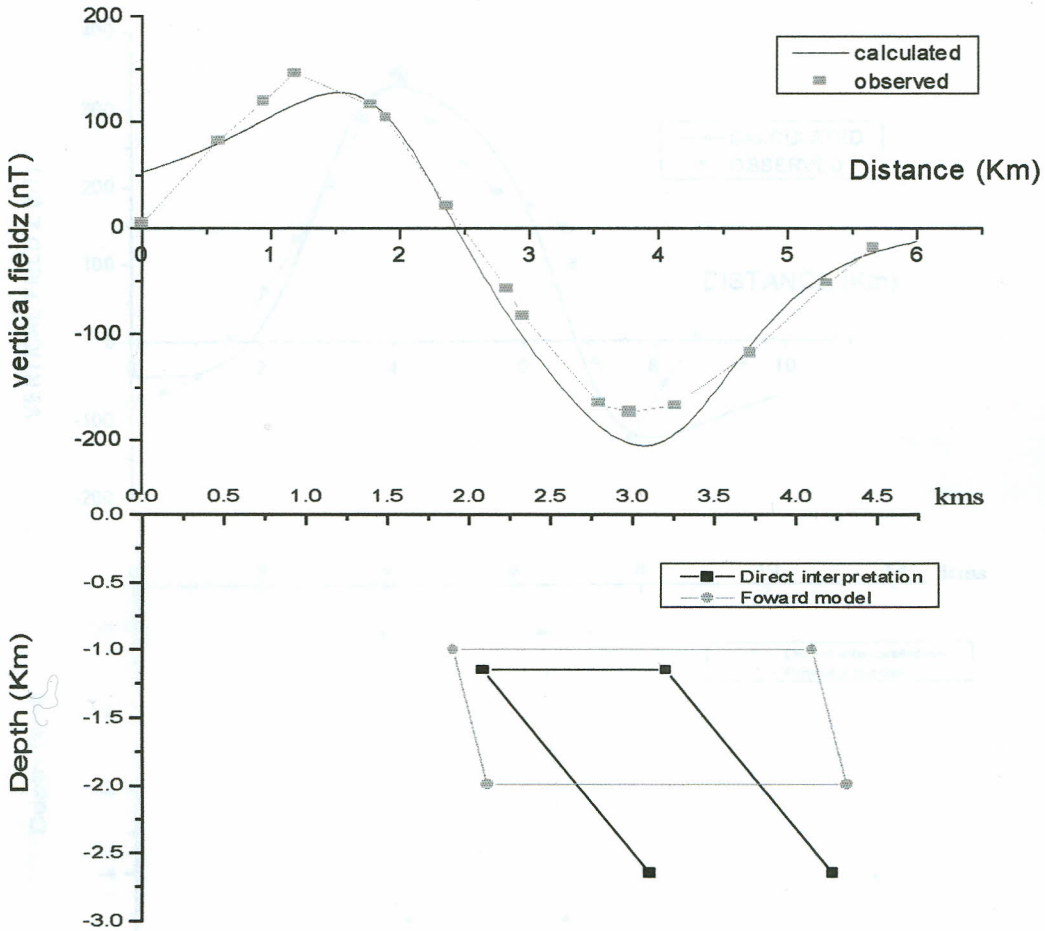

Figure 5.4(a) Calculated, observed anomaly, direct interpretation and forward model for 2-D body along profile P-Q.

Profile J-G

The magnetic profile J-G is oriented in the SSW-NNE direction bisecting the positive anomaly centred at the grid co-ordinates (197, 9783). The source body was modelled as a single body and parameters of the initial model altered to achieve a best fit. The fit obtained yielded the depth to the top of the body as 1.09 km, with a width of 3.5 km and a depth extent of 4.09 km. The magnetization of 2.0 AM^{-1} was attained with the modelled body dipping at an angle of 40° to the horizontal. The figure 5.4(b) shows the fit between

the observed and the computed anomalies along profile J-G together with the source body.

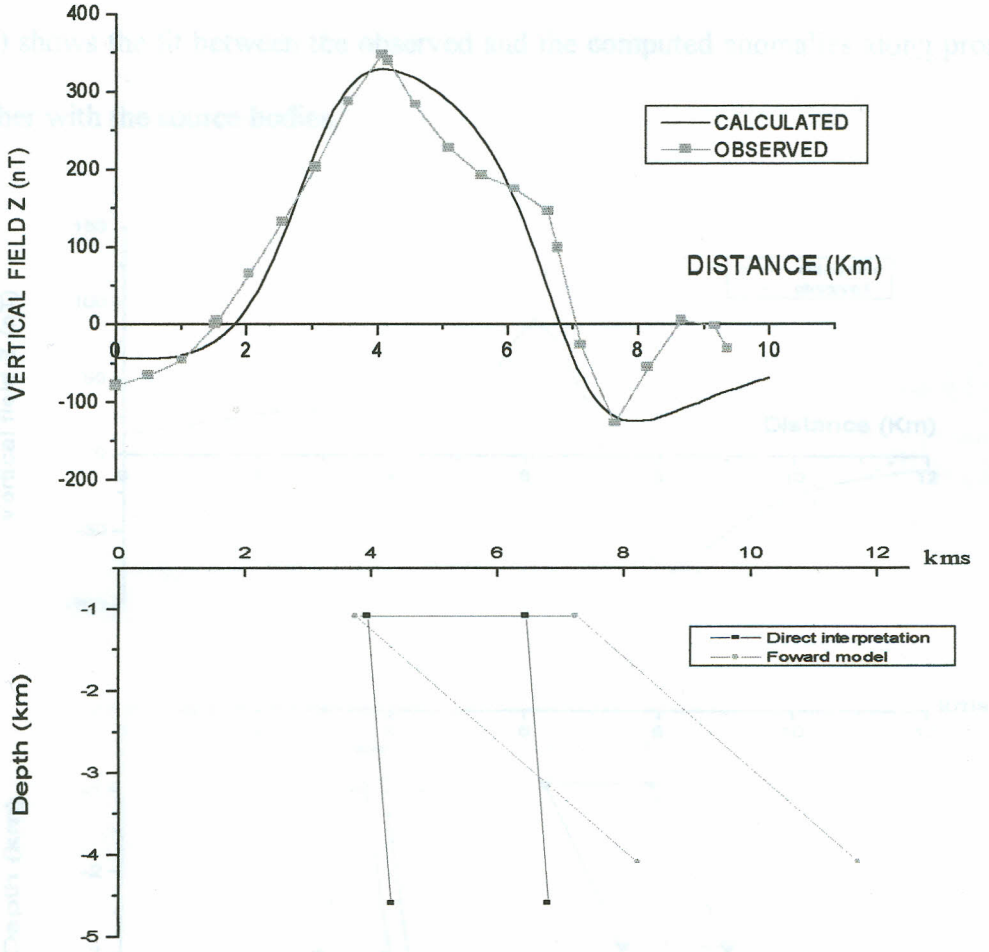

Figure 5.4(b) Calculated, observed anomaly, direct interpretation and forward model for 2-D body along profile J-G.

Profile R-S

The magnetic anomaly on profile R-S is in the NW-SE direction cutting through the two isolated negative anomalies centred at grid co-ordinates (198, 9789) and (200.5, 9787) respectively. In forward modelling, the magnetic anomaly in profile R-S is treated as being caused by two bodies. After altering the parameters to obtain the best fit, it was noted and 1.0 kms , with their widths being 1.57 kms and 1.0 kms and both their depth

extent being 2.9 kms respectively. They were modelled as both having a magnetization of 0.8 AM^{-1} and dipping at angles of 60° and 105° respectively to the horizontal. Figure 5.4(c) shows the fit between the observed and the computed anomalies along profile R-S together with the source bodies.

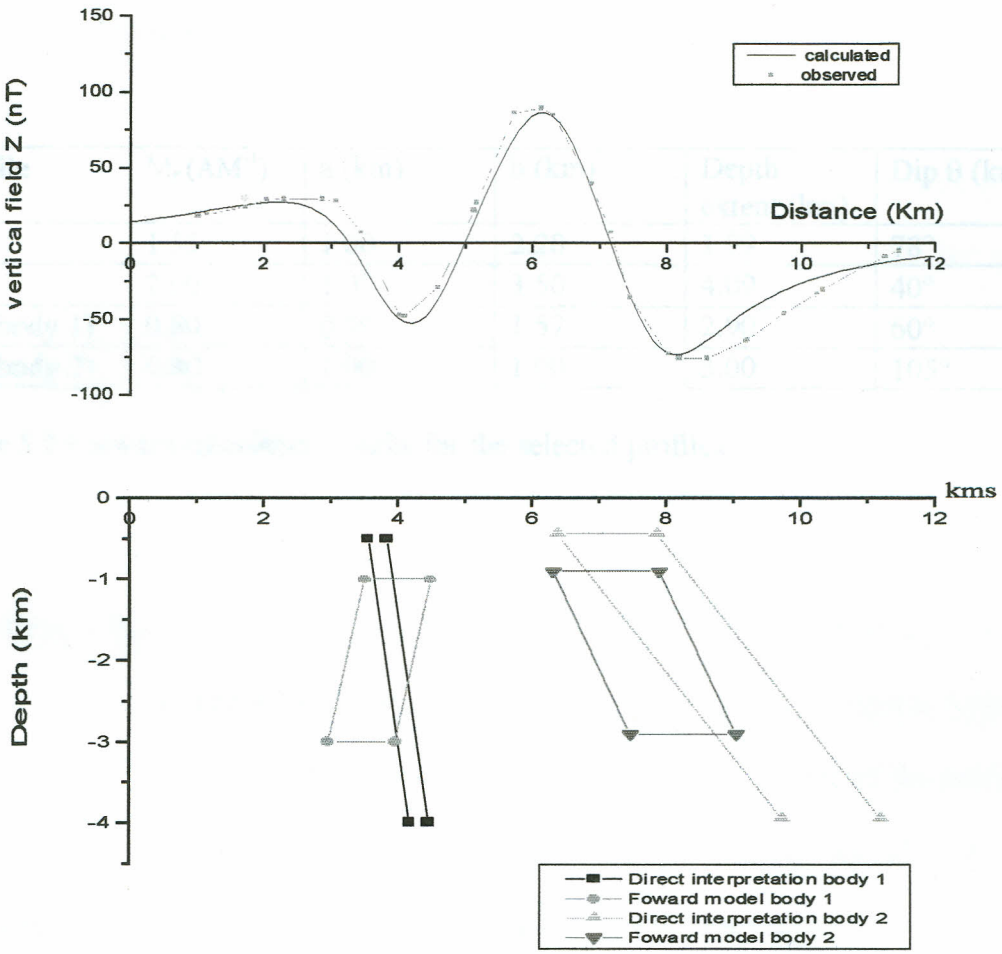

Figure 5.4(c) Calculated, observed anomaly, direct interpretation and forward model for 2-D body along profile R-S.

The results of forward modeling show different magnetization values of 1.55 AM^{-1}, 2.00 AM^{-1}, 0.80 AM^{-1}, and 0.80 AM^{-1}, widths of 2.20 km, 3.50 km, 1.57 km and 1.00 km, depth from the surface of 1.00 km, 1.09 km, 0.90 km, and 1.00km, depth extents of 1.99 km, 4.09 km, 2.90 km, and 3.00 km, dips of 78°,40°,60° and 105° for the three selected profiles. These results are summarized in table 5.2.

Profile	M_r (AM^{-1})	a (km)	b (km)	Depth extent (km)	Dip θ (km)
PQ	1.55	1.00	2.20	1.99	78°
JG	2.00	1.09	3.50	4.09	40°
RS (body 1)	0.80	0.90	1.57	2.90	60°
RS (body 2)	0.80	1.00	1.00	3.00	105°

Table 5.2 Forward calculation results for the selected profiles.

CHAPTER 6

6 SUMMARY AND CONCLUSION

6.1 Discussion

From the final results generated by forward modeling, the depth extent of the intrusives was determined. There are some variations of the fitted models from the results of the direct interpretation. From the results of both direct and forward modeling along profile PQ as shown in figure 5.4(a), there was a slight variation of depth to the top of the body and its dip but a remarkable difference on its thickness. Considering profile JG as in figure 5.4(b), the thickness of the body and depth from the top were stable but only the dip varies for both direct and forward calculation. For profile RS, there is a marked variation in the dip of body1 but the difference in dip for body2 is slight when using the direct and forward calculation as shown in figure 5.4(c). From the same figure, the thickness is more stable for body2 than for body1from the results of both techniques. The parameter, which is seen to be stable, is the depth to the top of the body as its variation for both direct and forward modeling is slight for all the profiles as in figures 5.4(a, b and c). Having used the results of direct interpretation as initial model for all the profiles, the magnetization values of bodies in profiles PQ, JG and RS (bodies 1 and 2) from forward modeling are 1.55 AM^{-1}, 2.0 AM^{-1}, 0.8 AM^{-1} and 0.8 AM^{-1} respectively. Comparing these to direct interpretation magnetization values which are 1.22 AM^{-1}, 1.26 AM^{-1}, 0.34 AM^{-1} and 0.43 AM^{-1} respectively, there is a higher difference for profile JG than for the other profiles. The depth to the bottom of the bodies along profiles PQ, JG, RS body 1 and RS body 2 are 1.99 km, 4.09 km, 3 km and 2.9 km respectively. These depths are considered shallow suggesting high temperature below the magnetic bodies. The bottom of the magnetic sources may be at a level corresponding to the Curie point isotherm where the

rocks cease to be magnetized. The magnetic anomaly along profile RS was modeled as consisting of two bodies both with a magnetization of 0.8 AM^{-1}. Direct interpretation yielded the magnetization of the bodies as 0.34 AM^{-1} and 0.43 AM^{-1} respectively. These anomalies occur in an area filled with lake beds and alluvium. The probable cause of these weak negative anomalies is suggested to be rocks eroded from a volcanic zone and weathered to form magnetized sediments.

The single body anomalies along profiles P-Q and J-G are not discernible in the airborne magnetic map figure 1.5. The anomaly along profile R-S was modeled as two bodies is also not seen in the same map. This may be because the resolution of individual anomalies from separate buried sources depends on the height of flight line above the level of the sources. Data obtained at lower elevation show more sharply defined and better resolved magnetic anomalies than those at greater heights (Dobrin,1988). The resolution is also affected by the magnetization intensity of the source body. The bodies along profile R-S were interpreted as having relatively low magnetization compared to anomalies along profiles P-Q and J-G.

The results of the analysis and modeling suggest that magnetic features, which had not been observed previously, underlie the study area. The magnetic anomalies along set profiles J-G and P-Q correlate well in position with the local gravity highs mapped in the Kenya Tertiary Rift Study (Beicip, 1987). By direct interpretation, these anomalies were found to have nearly the same magnetization intensity and from their dimensions of width, they were suggested to be prismatic intrusive. This is evident as from KRISP 90

seismic refraction investigation that the upper and middle crustal layers from eastern to western rift flank are mostly intruded by dikes and sills beneath the rift consisting of metamorphic basement rocks and an igneous mafic residuum accreted to the base of the crust derived from the upper mantle (Maguire *et al,* Braile *et al.,* 1994).

The anomalous bodies detected in this survey are smaller in size and with depth extents ranging from 1.99-4 km as compared to work due to Wolff (1992) in which the magnetic bodies detected in the area near Nguruman and Olorgesailie occur at depth extent range of 3.5-15 km. This may be an indication that the magma chambers were detected by Wolff (1992) but only volcanic dikes from such chambers were detected in this work. A 2-D software was used for modelling the bodies and hence the strike length was assumed to be infinity. This was a limitation since the finite strike length of the bodies could not be determined.

A cursory look at the geological map of Magadi figure 1.2 reveals that most of its area is thickly covered by volcanics of either central or fissural origin. Soil of any thickness is found only in the fault troughs which is filled by lake beds or alluvium. The lava surfaces are boulder stewn or rocky with only rare patches of yellow-brown silty soil. The spread lava fields in most of the area may have been as a result of injection of upper mantle material of high magnetic susceptibility into the fissured earth's crust.

The presence of shallow hot springs redistributed on the shores of the lake favours a model of relatively impermeable rocks forming a seal forcing escape of hot water from a

deep source at particular points. According to (Riaroh and Okoth, 1994), the springs issue from the base of fault scarps bounding the lake. The source of heat conducted to the underground water could be dike like intra-crustal structures penetrating from the magma chambers.

6.2 Conclusions and Recommendations

In this work, the magnetic prospecting method was found to be effective in detecting subsurface causative bodies suspected to be heat sources rooted from the asthenosphere. Simple magnetic bodies of prismatic shapes were modeled assuming uniform magnetization higher than the surrounding rock material The procedure in this work is useful only when the assumption of uniform magnetization is approximately true and if the results are not too dependent on shape of cross-section of the bodies.

The magnetic work carried out here cannot be regarded as an end but a valuable piece of work for further research and development. More geophysical and geological research needs to be intensified in this area for more findings. Further ground magnetic work is recommended especially in the southern region of the study area where an extended anomaly is visible from the aeromagnetic map figure1.5. This anomaly appear as isolated negative anomalies in this work but no conclusive remarks could be made since the data collected from this area was limited. Due to the non-unique nature of magnetic field data, for any given observed anomaly, there were multiple source body models matching the computed curves. The confidence level in the resultant model was dependent not only on

the degree of fit but also upon geologic and geophysical constraints employed during modeling. Such constraints included correlation to known surface geology.

REFERENCES

Abdullah A. Alshammari, 1985. Practical comparison between Doppler and G.P.S system, Surveying, instrumentation and Global Positioning System Vol 2 198c pp.226-234.

Baker, B.H., 1958. Geology of the Magadi area. Report Geological survey of Kenya 42.The Government printer, Nairobi.

Baker, B.H., 1963. Geology of the area south of Magadi. Report Geological survey of Kenya 61. The Government printer, Nairobi.

Baker, B.H. and Wohlenberg, J, 1971. Structure and evolution of the Kenya Rift Valley. Nature, 229: 538-542.

Baker, B.H., Mohr, P.A. and Williams, L.A.J., 1972. Geology of the Eastern Rift system of Africa. Geol. Soc. Am., special paper , 136, pp.67

Baker, B.H., Crossley. R. and Goles, G.G., 1978. Tectonic and magmatic evolution of the southern part of the Kenya Rift valley: in Petrology and Geochemistry of continental rifts, pp. 29-50.

Banks, R. and Beamish D., 1979. Melting in the crust and upper mantle beneath the Kenya Rift: evidence from geomagnetic deep sounding experiment. Geol. Soc. London. 136: 225-233.

Banks, R.J., Ottey, P., 1974.Geomagnetic deep sounding in and around the Kenya Rift valley. Geophys. J.R. Astron. Soc.36,pp. 321-335.

Beicip, 1987. Kenya Tertiary Rift study. Republic of Kenya, ministry of Energy and regional development p.p 39-40

Bonjer, K.P., Fuchs K., and Wohlenberg, J., 1970. Crustal structure of the East African Rift System from spectral response ratios of long period body waves .Z. Geophys., 36: 287 - 297.

Bowen, R., 1979. Geothermal resources. Applied science publishers ltd, pp. 22.

Braile, L.W., Wang, B., Daudt, C.R., Keller, G.R., Patel, J.P.,1994. Modeling the 2-D seismic velocity structure across the Kenya Rift. Tectonophysics 236, pp. 251-269.

Bullard, E.C (1949). The Magnetic field within the Earth. Proc. Roy. Soc. A, 197,433.

Chapman G.R., Lippard, S. and Martyn, J.E., 1978. The stratigraphy and structure of the Kamasia range, Kenya Rift Valley .J. Geol. Soc. London, 135: 265-281.

Compagnie Generale De Geophysique, 1987. A report to National Oil Corporation Of Kenya, Aeromagnetic Survey Of the Tertiary Rift Valley and Winam Gulf.

Clarke, M.C.G., Woodhall, D.G., Allen, D. and Darling, G., 1990. Geological, volcanological and hydrogeological controls on the occurrence of geothermal activity in the area surrounding Lake Naivasha Kenya. British Geological Survey report to the Ministry of Energy, Kenya, 138 p.p.

Crossley, R. and Knight, R.M., 1981. Volcanism in the Western Part of the Rift Valley in Southern Kenya. Bull. Volcanoes., 44: 117-128.

David G.S., 1981. Cambridge Encyclopedia of Earth Sciences. Cambridge University press, London.

Dobrin, M.B. and Savit, C.H., 1988. Introduction to Geophysical prospecting. McGraw-Hill Inc, NewYork. pp 706

Edcon, 1986. A report to ministry of Energy and regional development, Gravity and Magnetics pp.23-29.

Elsasser W.M. (1956). Hydro-Magnetic dynamo theory. Revs. Mod. Phys. ., 28, pp 135.

Fukushima N and Kaminde Y., 1973. Partial ring currents models for world-wide geomagnetic disturbances. Rev. Geophys. Space phys, 11 pp. 795-853.

Gregory, .W., 1921, The rift valleys and geology of East Africa: London, Seeley, Service 479 p.p.

Healey, J., 1975. Geothermal fields in zones of recent volcanism. Proc. Second U.N. Symp. Development and Use of Geothermal resources, San Francisco, Carlifornia., 415-422.

Henry, W.J., Mechie, J., Maguire, P.K.H., Khan, M.A. Prodehl, C., Keller, G.R and Patel, J., 1990. A Seismic Investigation of the Kenya Rift Valley. Geophys. J. Int., 10: 107-130

Hetzel, R. and Strecker, M.B., 1994. Late Mozambique belt structures in Western Kenya and their influence on the evolution of the cenozoic Kenya Rift. J. struct. Geol., 16: 189-201.

Hobson, G.D and Tiratsoo, E.N., 1985. Introduction to petroleum Geology, Gulf publishing Company Houston, Texas.

Keary,P and Brooks, M., 1984. An Introduction to Geophysical Exploration, ELBS edition pp.171-197.

Khan, M.A., and Swain, C.J., 1977. A catalogue of Gravity measurements in Kenya. Department of Geology, Leicester University pp.21-22.

KRISP Working group, 1987. Structure of the Kenyan rift from Seismic refraction. Nature, 325: 239-242.

KRISP working group, 1995. Lithosphere underneath southern Kenya. EOS 76,73, pp.81-82.

Maguire, P.K.H and Long, R.E., 1976. The structure of the Western flank of the Gregory Rift, Part 2. The Mantle. Geophys. J.R. Astron. Soc., 44: 677-688.

Mechie, J., Keller, G.R., Prodehl, c., Gachiri,S., Braile, L.W., Mooney, W.D., Gajewski, D. and Sandeier, J.K., 1994. Crustal structure beneath the Kenya rift from the axial profile data, in: Prodehl, C., Keller,G.R and Khan,M.A. (editors) crustal and upper mantle structure of the Kenya rift, Tectonophysics 236: 179-200

Mechie, J., Keller, G.R., Prodehl, C., Khan, M.A and Gachiri, S.J., 1996. A model for the structure, composition and evolution of the Kenya Rift, in: Fuchs, K., Altherr, R., Muller, B. and Prodehl, C. (editors), Stress and stress release in the lithosphere, Tectonophysics,278:

Militzer, H. and Weber, F., 1984. Angewandte Geophysik Bd.1, Gravimetrie und magnetik., Berlin(Akademie Verlag /Wien (Springer Verlag).

Morley, C.K., 1994. Interaction of deep and shallow processes in the evolution of the Kenya rift, In: Prodehl,c., Keller, G.R and Khan, M.A (editors), crustal and upper mantle structure of the Kenya rift, Tectonophysics 236: 81-92.

Morley, C.K., Wescott, W.A., Stone, D.M., Harper, R.M., Wigger, S.T., Karanja, F.M.,1992. Tectonic evolution of the northern Kenya Rift. J.Geol.Soc. London 149,pp 333-348.

Ndombi, J.M., 1978. Geology, gravity and resistivity studies of Olkaria geothermal field. Thesis (Ph.D) University of Stanford.

Nettleton, L.L., 1976 Gravity and Magnetic in oil prospecting. International series in the Earth and planetary sciences., Mc Graw-Hill, Inc. pp. 388.

Nyblande, A.A., and Pollack, H.N., 1992. A gravity model for the lithosphere in western Kenya and North eastern Tanzania. Tectonophysics, 212: 257-267.

Nyamweru, C., 1980. Rifts and Volcanoes. A study of the East-African Rift system. Nelson Africa, p.p. 81-82.

Parasnis, D.S., 1986 Principles of Applied Geophysics 1986, Chapman and Hall, U.S.A p.p. 14-29

Petrova G.N., Bobvov, V.N and Pudovkin M.I. 1980. Geomagnetism ,published under the auspices of UNESCO.

Riaroh, D., Okoth, W., 1994. The geothermal fields of the Kenya Rift. Tectonophysics 236: 117-130.

Riley, C., 1959, Saturation Prospecting- a new concept: CIMM Bulletin, V.52 p.p44 -46.

Rooney, D and Hutton, V.R.S., 1977. A magnetotelluric and magneto-variational study of the Gregory Rift Valley, Kenya. Geophys.J.R, Astron. Soc., 51:91-119.

Shackleton, R.M., 1986. Precambrian collision tectonics in Africa; in: Coward, M.P. and Ries, A.C (editors), collision Tectonics, Geological society special publication 19: 329-349.

Simpson, F., Haak, V. and Khan, M.A., 1997. The KRISP-94 magnetotelluric survey of early 1995: first results. Tectonophysics, 128.

Smith, M., 1994. Stratigraphic and structural constraints on mechanisms of active rifting in the Gregory Rift,Kenya, in ; Prodehl, C., Keller, G.R and Khan, M.A (editors), crustal and upper-mantle structure of the Kenya Rift, Tectonophysics, 236: 3-22.

Smith, M. and Mosley, P., 1993. Crustal heterogeinity and basement influence on the development of the Kenya Rift, East Africa Tectonics, 12:591-606.

Stacey, D.F., 1977. Physics of the Earth, 2nd edition , John Wiley and sons p.p 247

Swain, C.J., Khan, M.A., Wilton, T.J., Maquire ,P.K.H., and Griffiths, D.H., 1981. Seismic and gravity survey in the lake Baringo-Tugen hills area, Kenya Rift Valley.J.Geol.soc. London,138:93-102.

Vidal G., 1985. Analyse par te'le'de'tection et e'tude de terrain du Rift Est-Africain au Kenya: le proble'me du line'ament d' Assoua, The'se 3e'me cycle 262 p., Univ. Pierre et Marie Curie, Paris.

Ward. S.H., 1958, The role of geophysics in exploration in New Brunswick:C.I.MM Bulletin, March, P. 90-94.

Waring, G.A., revised by Blankenship, R and Bentall, R., 1965. Thermal springs of the United States and other countries in the world. U.S. Geol. Surv. Prof. Pap.492, pp 383.

White, R.S and Makenzie, D., 1989. Magmatism at rift zones: the generation of volcanic continental margins and flood basalts. J. Geophys. Res.,94: 7685-7729.

Williamson, K. H., 1975. Terrestrial heat flow studies in Kenya. Ph.D. Thesis, Univ. London pp 290

Wohlenberg, J. and Bhatt, N.V., 1972. A report on aeromagnetic surveys of two areas in the Kenya Rift Valley: Tectonophysics, 15/ 1,2 143-149.

Wolff. H., 1992. Interpretation Magnetischer Daten aus dem sudlichen Kenya Rift. Geologische Diplomabeit Vorgelegt Von pp.59.

APPENDIX 1

Conversion of Traverse Mercator grid co-odinates to latitudes/ longitudes.

X = Grid Easting (m) , Y = Grid Northing (m) , E_f = False Easting (m)

N_f = False Northing (m) ,V = Scale factor , λ_o = Central Meridian (radians) ,

λ = Longitude (radians) , φ = Latitude (radians).

Both the U.T.M and East Africa guide use the Clarke 1880 spheroid for which the following constants hold:

A = 6367386.5, B = 0.00256003, C = 0.0000273073 ,

E = 0.0068035= e^2 and R= 6378249.145 metres.

Where e is the eccentricity = $(1-b^2/a^2)$, a is the major semi axis and b is minor semi axis.

The meridional distance S is defined as :

$$S= A\varphi - AB \sin 2\varphi + AC \sin 4\varphi \qquad (R.1)$$

(i) Conversion of X,Y to λ,φ :

The meridional arc φ, must first be calculated using equation R.1 and successive approximations, thus:

$$\varphi_1 = (Y-N_f)/ AV = S/A \qquad (R.2)$$

$$\varphi_2 = \varphi_1 + B \sin 2\varphi_1 - C \sin 4\varphi_1 \qquad (R.3)$$

$$\varphi_3 = \varphi_2 + B \sin 2\varphi_2 - C \sin 4\varphi_2 \qquad (R.4)$$

Further iterations are possible, but the above will give an accuracy of better than 1 metre within 5° of the equator.

The formula for λ,φ are then:

$$\lambda = U/\cos\varphi_4 - (Q + 2 \tan^2\varphi_4) U^3/ (6\cos\varphi_4) + \lambda_0 \qquad (R.5)$$

$$\varphi_4 = \varphi_3 - \tan\varphi_3 z^2/ 2T \qquad (R.6)$$

Where,

$$P = 1 - E\sin\varphi_3 \quad \text{(R.7)}$$

$$Q = P/(1-E) \quad \text{(R.8)}$$

$$T = R^2/PQ \quad \text{(R.9)}$$

$$Z = (X - E_f)/V \quad \text{(R.10)}$$

$$U = Z\sqrt{P}/R \quad \text{(R.11)}$$

(ii) Conversion of λ,φ to X,Y

Using equations (1) , (4) and (5),

$$X = (RV/\sqrt{P})(\cos\varphi(\lambda-\lambda_0) + (Q-\tan^2\varphi)\cos^3\varphi(\lambda-\lambda_0)^3/6) + E_f \quad \text{(R.12)}$$

$$Y = SV + (RV/\sqrt{P})\sin\varphi\cos\varphi(\lambda-\lambda_0)^2 + N_f \quad \text{(R.13)}$$

Reference: (Khan and Swain, 1977)

APPENDIX 2

The appendix 2 displays all all the data recorded in all the 53 stations established in the study area. This includes the station code, the position co-ordinates of the stations both in degrees and in rectangular co-ordinates, the four magnetic readings from a station together with their average, the base magnetic reading interpolated for a particular station at the time the magnetic field was read and the residual magnetic intensity in a station including its standard deviation from the average and the standard error. This is displayed as in table A1 below.

STATION	LAT/DEG	LON/DEG	GRID-E	GRID N	MAG1	MAG2	MAG3	MAG4	MAG AV	MAG BAS	MAG RES	S.E ±
AC1	-1.89608	36.29033	198.53	9790.21	-15274	-15275	-15275	-15273	-15274.3	-15300.3	26	0.4787
A2	-1.89723	36.30318	199.96	9790.08	-15169	-15170	-15175	-15171	-15171.3	-15306	134.75	1.315
A3	-1.9043	36.3049	200.15	9789.3	-15030	-15032	-15030	-15031	-15030.8	-15280	249.2	0.4787
A4	-1.9187	36.304	200.05	9787.7	-15104	-15108	-15106	-15109	-15106.8	-15281	174.2	1.1087
A5	-1.9264	36.3089	200.6	9786.85	-15172	-15173	-15173	-15174	-15173	-15290.3	117.25	0.4083
A6	-1.93021	36.3129	200.85	9785.65	-14952	-14953	-14949	-14954	-14952	-15297	345.25	1.0801
A7	-1.83533	36.32219	202.06	9796.94	-15026	-15025	-15024	-15025	-15025	-15270	245	0.4083
A8	-1.85098	36.31727	201.52	9795.2	-15028	-15033	-15031	-15029	-15030.3	-15290	259.7	1.1087
AM9	-1.87213	36.31243	200.75	9792.9	-14946	-14948	-14946	-14948	-14947	-15265	318	0.5773
A10	-1.8808	36.3049	200.15	9791.9	-15009	-15012	-15011	-15012	-15011	-15269	258	0.7071
A11	-1.9007	36.29441	198.98	9789.7	-15149	-15146	-15148	-15146	-15147.3	-15411.5	264.2	0.75
A12	-1.909	36.29401	198.94	9788.78	-15112	-15115	-15112	-15113	-15113	-15414	301	0.7071
A13	-1.91944	36.29371	198.91	9787.62	-15052	-15050	-15051	-15050	-15050.8	15408.8	318	0.4787
A14	-1.93059	36.29288	198.82	9786.39	-15093	-15092	-15093	-15092	-15092.5	-15410	317.5	0.2887
A15	-1.94095	36.29222	198.75	9785.24	-15179	-15175	-15180	-15179	-15178.3	-14409.5	231.2	1.1087
A16	-1.95051	36.29216	198.74	9784.19	-15246	-15247	-15243	-15246	-15245.5	-15409.5	164	0.866
A17	-1.966	36.29054	198.56	9782.47	-15126	-15126	-15121	-15121	-15123.5	-15410	286.5	1.4434
A18	-1.89	36.3103	200.75	9790.88	-15105	-15105	-15104	-15106	-15105	-15305	200	0.4083
A19	-1.895	36.3197	201.8	9790.33	-15016	-15015	-15018	-15015	-15016	-15304	288	0.7071
A20	-1.8941	36.3269	202.6	9790.43	-15009	-15006	-15005	-15008	-15007	-15338	331	0.9129
A21	-1.8944	36.3438	204.48	9790.4	-14959	-14957	-14954	-14958	-14957	-15326	369	1.0801
A22	-1.8871	36.3052	200.18	9791.2	-15036	-15039	-15037	-15043	-15038.8	-15293	254.2	1.5478
A23	-1.86135	36.3157	201.35	9794.06	-15025	-15027	-15028	-15027	-15026.8	-15270	243.2	0.6292
A24	-1.8586	36.3104	200.75	9794.35	-15087	-15094	-15090	-15091	-15090.5	-15275	184.5	1.4434
A25	-1.8586	36.3209	201.93	9794.35	-14784	-14788	-14783	-14784	-14784.8	-15215	430.2	1.1087
A26	-1.8587	36.3328	203.25	9794.35	-14863	-14861	-14864	-14861	-14862.3	-15307	444.7	0.75
A27	-1.8691	36.3314	203.1	9793.2	-14522	-14516	-14517	-14518	-14518.3	-15292	773.7	1.315
A28	-1.8398	36.3036	200	9796.43	-14913	-14915	-14915	-14913	-14914	-15297	383	0.5774
A29	-1.8411	36.3412	204.18	9796.3	-14710	-14710	-14709	-14708	-14709.3	-15315	605.7	0.4787
B1	-1.90769	36.28736	198.2	9788.92	-15271	-15272	-15270	-15273	-15271.5	-15271.5	0	0.6455
BM2	-1.9222	36.28622	198.07	9787.32	-15190	-15187	-15186	-15189	-15188	-15460	272	0.9129
BM3	-1.93935	36.28172	197.58	9785.42	-14971	-14968	-14966	-14966	-14967.8	-15341	373.2	1.1815
B4	-1.95515	36.2774	197.1	9782.82	-14890	-14892	-14886	-14888	-14889	-15370	481	1.291
B5	-1.97718	36.27828	197.2	9781.23	-15144	-15145	-15139	-15140	-15142	-15354.5	212.5	1.472
B6*	-1.98188	36.28358	197.79	9780.71	-9558	-9560	-9558	-9556	-9558	-15359	5801	0.8165
B60*	-1.97742	36.27968	197.36	9781.17	-15302	-15305	-15306	-15302	-15303.8	-15323.8	20	1.0308
B61*	-1.97829	36.28107	197.51	9781.11	-15346	-15344	-15347	-15345	-15345.5	-15225	-120.5	0.6455
B62*	-1.9785	36.28227	197.64	9781.09	-15722	-15718	-15720	-15718	-15719.5	-15322.5	-397	0.9575
B63*	-1.97898	36.28352	197.78	9781.04	-15663	-15661	-15659	-15656	-15659.8	-15323.6	-336.2	1.4931
B64*	-1.97859	36.28353	197.79	9781.08	-15668	-15664	-15664	-15663	-15664.8	-15324	-340.8	1.1087
B7	-1.96547	36.28018	197.79	9780.71	-14939	-14937	-14933	-14933	-14935.5	-15300	364.5	1.5
B8	-1.99269	36.25921	195.08	9779.51	-15371	-15370	-15372	-15368	-15370.3	-15285	-85.25	0.8539
B9	-1.93047	36.28387	197.81	9786.4	-15344	-15343	-15339	-15341	-15341.8	-15360	18.2	1.1087
B10	-1.91237	36.28649	198.1	9788.41	-15105	-15104	-15104	-15100	-15103.3	-15340	236.7	1.1087
B11	-1.98672	36.26926	196.2	9780.18	-15356	-15358	-15355	-15353	-15355.5	-15375	19.5	1.0408
B12	-1.99988	36.24993	194.05	9778.72	-15547	-15545	-15544	-15544	-15545	-15371.5	-173.5	0.7071
B13	-2.01095	36.24399	193.39	9777.49	-15458	-15457	-15456	-15459	-15457.5	-15369.5	-88	0.6455
B14	-2.02	36.23462	192.35	9776.49	-15418	-15416	-15415	-15415	-15416	-15331.8	-84.2	0.7071
B15	-2.03289	36.22832	191.65	9795.06	-15470	-15468	-15464	-15464	-15466.5	-15333.5	-133	1.5
B16	-2.04478	36.22243	190.99	9773.74	-15417	-15418	-15421	-15422	-15419.5	-15335.5	-84	1.1902
C2	-1.88229	36.28361	197.78	9791.73	-14988	-14992	-14990	-14990	-14990	-15305	315	0.8165
C3	-1.88087	36.27673	197.01	9791.89	-14945	-14946	-14946	-14947	-14946	-15267	321	0.4083
C4	-1.88032	36.26596	195.81	9791.95	-15028	-15025	-15024	-15026	-15025.8	-15250.8	225	0.8539

Table A.1. Position co-ordinates and vertical magnetic field data.